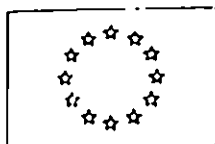
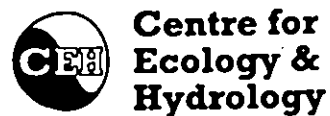


1997/026

Physiologically-based models of semi-arid vegetation dynamics for improved description of land surface/atmosphere interactions in climate models

Final report (ENV4-CT95-5007)
Reporting period: January 1996-December 1997

A. Verhoef
Institute of Hydrology
Wallingford, UK



*Commission of the European Communities
Directorate-General XII
Science, Research and Development*

CONTENTS

SUMMARY OF ACHIEVEMENTS AND MAIN CONCLUSIONS	2
OBJECTIVES OF THE TRAINING ACTIVITIES	3
DESCRIPTION OF RESULTS OBTAINED DURING THE TRAINING PERIOD	4
1. INTRODUCTION	4
2. THEORY	6
2.1. SVAT description	6
2.2. Growth model	10
2.3. Soil heat and moisture transport	12
3. MATERIAL AND METHODS	17
3.1. Description of field site and conditions	17
3.2. Environmental driving and verification data	17
3.3. Model parameters	20
3.4. Optimisation of photosynthesis-leaf conductance model	22
3.5. Parameterisation of soil respiration	23
3.6. Water use efficiency	23
3.7. Procedure for sensitivity analysis	23
4. RESULTS	24
4.1. Least squares fitting procedure	24
4.2. The energy balance and net CO ₂ flux	24
4.3. Surface temperatures	25
4.4. Predictions of component fluxes and surface temperatures	27
4.5. Water use efficiency	28
4.6. Verification of the extended SVAT	28
4.7. Sensitivity analysis	30
5. DISCUSSION	32
6. CONCLUSIONS	37
ACKNOWLEDGEMENTS	38
APPENDIX 1	39
REFERENCES	41
UNEXPECTED DEVELOPMENTS, RESULTS OR CONCLUSIONS NOT FORESEEN AT THE ONSET OF THE TRAINING PERIOD	47
RESEARCH LINES AND/OR RESEARCH APPROACHES WHICH PROVED TO BE UNSUCCESSFUL	47
PUBLICATIONS	47



RESEARCH PROGRAMME IN THE FIELD OF ENVIRONMENTAL PROTECTION

SECTORIAL GRANTS

FINAL REPORT

- Contract n°: ENV4-CT95-5007
- Name of trainee: Dr. VERHOEF Anne
- Reporting period: 1-1-1996 until 31-12-1997
- Period covered by the training contract: 1-1-1996 until 31-12-1997
- Name of scientific supervisor and address of host laboratory:

Dr. ALLEN Simon

Institute of Hydrology

Crowmarsh Gifford

Wallingford - Oxfordshire - OX10 8BB

United Kingdom



1) SUMMARY OF ACHIEVEMENTS AND MAIN CONCLUSIONS

A Soil Vegetation Atmosphere Transfer scheme (SVAT), describing the fluxes of heat, water vapour and CO₂ between a multi-component vegetated land surface and the atmosphere, has been developed. The parameterisation of leaf conductance is based on a physiological photosynthesis-conductance model (Jacobs *et al.* 1996). The energy partitioning between the various components is calculated using the Penman-Monteith equation and a resistance network based upon a generalisation of a two-component model, for a simplified savannah of shrubs and a herbaceous understorey, described by Huntingford *et al.* (1995). The SVAT has been calibrated and tested using 1 month of micrometeorological and physiological measurements collected over a sparse savannah in the Sahel. The model explicitly represents the four major functional components of the savannah: shrubs (C₃ photosynthesis), grasses (C₄), herbs (C₃) and bare soil. The leaf conductance model for the shrub, grass and herb components was calibrated against porometry measurements made in the field.

The performance of the SVAT was tested against independent surface flux and temperature measurements. Agreement between the model predictions and measurements of the sensible and latent heat fluxes, net CO₂ exchange and surface temperatures is good: in all cases at least 80% of the variance in the measurements is explained by the model. Separate flux and surface temperature predictions for the four surface components were satisfactory, although complete verification was difficult as data were lacking for some variables. Predicted water use efficiency (*WUE*) of the vegetation showed a strong, non-linear dependence on vapour pressure deficit, especially for the bushes and the grasses. *WUE* for the grasses was about 3 times as large as found for the bushes and herbs.

This calibrated SVAT has been extended by incorporating a simple growth model, which allows for leaf area index to be calculated from CO₂ uptake instead of using measured values. The extended SVAT also contains a multi-layer soil model to estimate soil heat fluxes (the original model employed measured values). It therefore only requires micrometeorological data at reference level and hence can be easily used to investigate the likely effects of climate change and CO₂ enrichment on evaporation and CO₂ uptake. For this purpose the model was run for four different scenarios: a reference model run (original micrometeorological input), a run with doubled atmospheric CO₂ concentration, a run with increased air temperature (+ 1.5 °C), and a final run in which both driving variables were increased. It appeared that doubling the atmospheric CO₂ concentration (with or without a temperature increase) had the largest effect: it decreased total evaporation by about 20% and roughly doubled the net CO₂ uptake for the savannah. Interestingly, the different components made a significantly different contribution to these changes in the total flux.

These simulations are considered to be more reliable than those done in the past where empirical descriptions of leaf conductance were employed, often without taking into account the effect of CO₂ concentration, and where measured values of leaf area index were used. The multi-component, mechanistic model described in this report, if necessary linked to a meso-scale or GCM model, will be a valuable tool for understanding the competition between different species in a plant community during global climate change.

2) **OBJECTIVES OF THE TRAINING ACTIVITIES** (maximum 10 lines):

The work proposed will combine plant physiological models of leaf surface conductance and vegetation growth with an existing (two-layer) Soil-Vegetation-Atmosphere-Transfer (SVAT) model (the IH 'Mitre' scheme) describing evapotranspiration. This will produce a CO₂ responsive fully interactive scheme, which, if included in a GCM, will improve the accuracy of climate predictions, especially for multi-component ecosystems.

3) DESCRIPTION OF RESULTS OBTAINED DURING THE TRAINING PERIOD:

1. INTRODUCTION

The model parameterisation of the vegetated land surface/atmosphere interaction is known as a Soil Vegetation Atmosphere Transfer scheme (SVAT). The SVATs presently implemented in meso-scale models or GCMs are often simplified representations of reality (e.g. Deardorff 1978; Sellers *et al.* 1986), and lagging behind current knowledge of the processes and the surface properties, especially of the leaf stomatal resistance.

Laboratory and field studies have shown that stomata respond in a complex way to environmental variables such as light intensity, humidity and atmospheric CO₂ concentration and to plant and soil water status. The SVAT schemes of most current GCMs either do not represent this behaviour, by using a fixed surface conductance for each type of vegetation, or rely on empirical response functions (Sellers *et al.* 1986). In particular, the response to CO₂ is not represented, despite the large amount of experimental evidence supporting its existence (Rozema *et al.* 1993). Plant physiological measurements and modelling suggest that as atmospheric CO₂ concentration rises, vegetation will respond with increased CO₂ uptake, and reduced transpiration, affecting the land surface energy balance, and hence climate, through changes in surface conductance and soil moisture content. An important feedback process is therefore being omitted from many current GCM studies of the impact of increased CO₂ on climate, undermining the credibility of global and regional predictions.

Consequently, improving the parameterisation of the leaf stomatal conductance has received a great deal of attention lately. There is a tendency to replace the empirical approach, in which stomatal behaviour is modelled in terms of independently acting environmental factors, by the physiological approach. The latter combines models of stomatal behaviour and photosynthesis (Ball *et al.* 1987; Leuning 1995; Harley & Baldocchi 1995; Jacobs *et al.* 1996) and allows feedback between surface variables and fluxes. An added advantage of this physiological parameterisation is that as well as giving values of leaf conductance, it also provides estimates of CO₂ exchange between the vegetation and the atmosphere.

Furthermore, modellers realized that the single-component Big Leaf model described by the Penman-Monteith equation (Monteith 1965) only has a limited validity, because many of the world's biomes are sparse (without canopy closure), heterogeneous (consisting of functionally different components, e.g. trees and herbs) or both. These systems can only be satisfactorily described by multi-component descriptions (e.g. Shuttleworth & Wallace 1985; Choudhury & Monteith 1988), where the different plant types and the soil are explicitly represented. However, the vast majority of these multi-component SVAT models only allows for two sources, usually a main canopy with a bare soil substrate or vegetated understorey (see Dolman 1993; Huntingford *et al.* 1995).

This report describes a multi-component SVAT which addresses the concerns outlined above. It simulates the energy balance of the entire plant-soil system and of its

components, as well as the photosynthesis of the canopy and various types of understorey (e.g. C₃ herbs and C₄ grasses), and the heterotrophic (soil) respiratory efflux of CO₂, which is assumed to be largely determined by soil temperature and soil moisture content (see e.g. Norman *et al.* 1992). The scheme was developed to describe a sparsely vegetated Sahelian savannah, consisting of four components (i.e. shrubs, herbs, grasses and bare soil), but the equations are generally applicable and could be extended to a larger number of components. The calibration of the model and its accuracy in predicting measured fluxes of sensible heat, latent heat and CO₂, and surface temperatures for the total savannah and its separate components are presented. We also calculated the water use efficiency of the three vegetated components, to illustrate how this scheme can provide useful physiological parameters, which could be used for practical purposes, such as modelling the growth of agroforestry systems.

Furthermore, the calibrated SVAT has been used to investigate the likely effects of climate change and CO₂ enrichment on evaporation and CO₂ uptake. This was done by incorporating a module describing soil heat and moisture transport (previously, measured values of soil heat flux and soil moisture content were used), as well as a simple growth model, that allowed for changes in leaf area index with changes in CO₂ uptake. For this kind of sensitivity study the model provides a powerful tool, because it simultaneously describes the energy balance, CO₂ exchange and leaf conductance of the vegetation components. In this way it allows for interactions and feedbacks between the four different components of this savannah ecosystem and the atmosphere. A study like this in which all the vegetation components are lumped into one source, would undoubtedly lead to inaccurate and unreliable results.

2. THEORY

2.1. SVAT description

Total latent heat flux, λE (W m^{-2}), from a surface consisting of i components, each with fractional coverage α_i ($\sum_i \alpha_i = 1.0$), can be written as (see Dolman 1993; Huntingford *et al.* 1995):

$$\lambda E = \sum_i \alpha_i PM_i Y_i \quad (1)$$

with λ the latent heat of vaporisation (J kg^{-1}) and PM_i and Y_i the Penman-Monteith and resistance combination terms for component i , respectively.

The PM_i terms are given by

$$PM_i = \Delta A + \frac{(\rho C_p D_r - \Delta r_{c,i} (A - A_i))}{r_{a,a} + r_{c,i}} \left[\Delta + \gamma \left(\frac{r_{a,a} + r_{a,i} + \mu r_{b,i}}{r_{a,a} + r_{c,i}} + \frac{r_{s,i}}{r_{a,a} + r_{c,i}} \right) \right] \quad (2)$$

with $r_{a,a}$ (s m^{-1}) the atmospheric aerodynamic resistance between the canopy source height (level of mean canopy flow) and atmospheric reference level z_r (m), $r_{c,i}$ (s m^{-1}) the total aerodynamic resistance between surface i and the canopy source height, $r_{a,i}$ the within-canopy aerodynamic resistance (s m^{-1}), $r_{b,i}$ the bulk boundary layer resistance (s m^{-1}) and $r_{s,i}$ (s m^{-1}) the surface resistance for each component i . A (W m^{-2}) is the available energy for the whole system, whereas A_i (W m^{-2}) denotes the available energy for the i components, which is the difference between net radiation, $R_{n,i}$ (W m^{-2}) and soil heat flux G_i (W m^{-2}). D_r (mbar) is the vapour pressure deficit at reference level. Δ (mbar K^{-1}) is the slope of the vapour pressure temperature curve, γ is the psychrometric constant (mbar K^{-1}), ρ (kg m^{-3}) is the density of air and C_p ($\text{J kg}^{-1} \text{K}^{-1}$) is the specific heat of air at constant pressure. The constant μ can vary between 1 (amphistomatous leaves or soil) and 2 (hypostomatous leaves). If $\mu = 1$, the denominator in Eqn 2 will have its familiar form of $\left[\Delta + \gamma \left(1 + \frac{r_{s,i}}{r_{a,a} + r_{c,i}} \right) \right]$.

For the savannah, four surface components are distinguished: bushes, herbs, grasses and bare soil as denoted with the subscripts $i = b, h, g$ and s . A schematic diagram of the resistance network for the model and its major variables is given in Fig. 1. Atmospheric variables at the canopy source height are denoted by the subscript 0, whereas at the reference and surface level the subscripts r and s have been used, respectively. The coverages of the shrubs, understory and bare soil are not allowed to overlap. Furthermore, bare soil applies to extensive patches not overshadowed by any plants.

The total aerodynamic resistances between the surfaces and the canopy source height, $r_{c,i}$, are given by $r_{c,b} = r_{b,b}$, $r_{c,h} = r_{a,h} + r_{b,h}$, $r_{c,g} = r_{a,g} + r_{b,g}$ and $r_{c,s} = r_{a,s}$. These resistances, together with the atmospheric aerodynamic resistance $r_{a,a}$, are calculated using the parameterisations given in Huntingford *et al.* (1995), while $r_{a,s}$ is set to a constant value of 100 s m^{-1} , following preliminary tests with the model.

The in-canopy aerodynamic resistance for the undergrowth (mixture of herbs and grasses) is given by

$$r_{a,h} = r_{a,g} = \frac{e^n h_b}{nK(h_b)} \left[e^{-nz_u/h_b} - e^{-nz_b/h_b} \right] \quad (3)$$

with n the decay coefficient (-), h_b the canopy height of the bushes (m), and $K(h_b)$ the eddy diffusivity at the top of the bushes ($\text{m}^2 \text{s}^{-1}$). Parameters $z_b (= z_{0m,b} + d_b)$ and $z_u (= z_{0m,u} + d_u)$ are the momentum sink height (m) for the bushes and undergrowth, respectively. Here, $z_{0m,b}$ and $z_{0m,u}$ and d_b and d_u are the roughness lengths and displacement heights for the bushes and undergrowth (m), respectively.

The bulk boundary layer resistances are found from

$$r_{b,i} = \frac{70 \left(\frac{l_i}{u_i} \right)^{0.5}}{L_i^*} \quad (4)$$

with L_i^* (m^2 leaf m^2 ground area) the local leaf area for component i , i.e. the leaf area index a vegetation component would have if it wholly covered the surface, l_i (m) the leaf width of vegetation type i and u_i (m s^{-1}) is given by $u_i = u_b e^{n(z_i/h_b - 1)}$, with $z_i = z_b$ or z_u , and u_b (m s^{-1}) the windspeed at bush canopy height. The units of the constant 70 in Eqn 4 are $\text{s}^{1/2} \text{m}^{-1}$.

The aerodynamic resistance between the canopy source level and the atmospheric reference level is obtained from

$$r_{a,a} = \frac{1}{\kappa u} \left[\ln \frac{z_r - d}{h_b - d} - \Psi_h(z_r) + \Psi_h(h_b) \right] + \frac{h_b}{nK(h_b)} \left[e^{n(1 - z_b/h_b)} - 1 \right] \quad (5)$$

with u , the friction velocity (m s^{-1}), κ the Von K arm an constant, d the zero plane displacement for the total surface (m) and $\Psi_h(z)$ the integrated stability correction to eddy diffusivity for heat and water vapour at height z . The friction velocity is found from

$$u_* = \frac{\kappa u_r}{\ln((z_r - d) / z_{0m}) - \Psi_m(z_r - d)} \quad (6)$$

with $\Psi_m(z)$ the integrated stability correction to eddy diffusivity for momentum at height $z_r - d$, u_r the windspeed at reference height (m s^{-1}) and z_{0m} (m) the roughness length for momentum for the total surface.

The canopy surface resistances for water vapour are calculated from $r_{s,i} = r_{l,i} / L_i^*$, where the calculation of the leaf stomatal resistance, $r_{l,i}$ (s m^{-1}), is based on a mechanistic model (Jacobs *et al.* 1996) which uses the relationship between the net photosynthetic rate of plants, $P_{n,i}$ (mg m^{-2} leaf s^{-1}) and leaf stomatal resistance:

$$r_{l,i} = (C_{s,i} - C_{i,i}) / 1.6 f_0 P_{n,i} \quad (7)$$

Here, $C_{s,i}$ and $C_{i,i}$ (mg m^{-3}) are the leaf surface and internal CO_2 concentration for vegetation component i , respectively, and f_0 is a linear multiplication factor, added in this study, which is dependent on soil moisture status (see Eqn A10). $r_{l,i}$ (and $P_{n,i}$) is also dependent on absorbed PAR radiation, $I_{a,i}$ (W m^{-2}), surface temperature $T_{s,i}$ ($^\circ\text{C}$) and surface vapour pressure deficit $D_{s,i}$ (mbar) as described in Appendix 1.

The soil surface resistance, $r_{s,s}$, is dependent on day number (Verhoef 1995), which resulted in values for $r_{s,s}$ ranging between 1000 and 10000 s m^{-1} .

The Y_i terms in Eqn 1 are found from equations analogous to those given in the Appendix of Huntingford *et al.* (1995):

$$Y_b = W_h W_g W_s (W_b + W_a) / X \quad (8a)$$

$$Y_h = W_b W_g W_s (W_h + W_a) / X \quad (8b)$$

$$Y_g = W_b W_h W_s (W_g + W_a) / X \quad (8c)$$

$$Y_s = W_b W_h W_g (W_s + W_a) / X \quad (8d)$$

with $W_a = (\Delta + \gamma)r_{a,a}$, $W_i = (\Delta + \mu\gamma)r_{c,i} + \gamma r_{s,i}$, with $i = b, h, g$ and s and

$$X = W_b W_h W_g W_s + \alpha_b W_h W_g W_s W_a + \alpha_h W_b W_g W_s W_a + \alpha_g W_b W_h W_s W_a + \alpha_s W_b W_h W_g W_a. \quad (9)$$

The available energy for each component ($A_{n,i} = R_{n,i} - G_i$) is found by calculating net radiation for each component i from

$$R_{n,i} = (1 - a_i)R_{sol} + R_{l,i} - \varepsilon_i \sigma T_{s,i}^4 - (1 - \varepsilon_i)R_{l,d} \quad (10)$$

while G_b , G_h , G_g and G_s are obtained from the measured values of soil heat flux. In Eqn 10, a_i and ε_i are the albedo and emissivity for component i , R_{sol} is the incoming solar radiation (W m^{-2}), $R_{l,i}$ is the incoming longwave radiation (W m^{-2}), and $T_{s,i}$ ($^\circ\text{C}$) is the surface temperature for component i (for its calculation see Eqn 14a). In the field, the herbs and grasses were intimately mixed to form a more or less uniform understorey, hence a means of partitioning the net radiation was required. Therefore, the net radiation of the herbs and the grasses is multiplied by L_i / L_u , where L_i denotes the component leaf area index ($\text{m}^2 \text{m}^{-2}$), with $i = h$ or g and L_u the total leaf area index for the undergrowth (i.e. herbs plus grasses). Total net radiation and total available energy are found from $R_n = \sum_i \alpha_i R_{n,i}$ and $A = \sum_i \alpha_i A_i$, respectively.

With λE found from Eqn 1, the vapour pressure deficit at the canopy source level (in mbar) is

$$D_0 = D_r + \left\{ \Delta A - (\Delta + \gamma) \lambda E \right\} r_{a,a} / \rho C_p \quad (11)$$

with the symbols as described above. At this same level, the temperature T_0 ($^\circ\text{C}$), and vapour pressure e_0 (mbar) can be obtained from

$$T_0 = \left((A - \lambda E) r_{a,a} / \rho C_p \right) + T_r \quad (12a)$$

$$e_0 = e_s(T_0) - D_0 \quad (12b)$$

in which $e_s(T_0)$ is the saturated vapour pressure at canopy source level temperature (mbar) and T_r is the reference level air temperature ($^{\circ}$ C).

With knowledge of D_0 , evapotranspiration from the four component surfaces can be calculated from

$$\lambda E_i = \left[\Delta A_i + \frac{\rho C_p D_0}{r_{c,i}} \right] / \left[\Delta + \gamma \left(\left(\frac{r_{a,i} + \mu r_{b,i}}{r_{c,i}} \right) + \frac{r_{s,i}}{r_{c,i}} \right) \right] \quad (13)$$

Surface temperatures for the four components are then found from

$$T_{s,i} = T_0 + \left((A_i - \lambda E_i) r_{c,i} \right) / \rho C_p \quad (14a)$$

and surface values of D using

$$D_{s,i} = \left(e_s(T_{s,i}) - e_0 \right) / \left(1 + \mu \frac{r_{c,i}}{r_{s,i}} \right) \quad (14b)$$

with $e_s(T_{s,i})$ the saturated vapour pressure at surface temperature (mbar).

The total net CO_2 flux (positive downwards) is calculated using:

$$F_c = \alpha_b L_b P_{n,b} + \alpha_h L_h P_{n,h} + \alpha_g L_g P_{n,g} - R_{\text{soil}} \quad (15)$$

In Eqn 15, R_{soil} is the total respiration of soil and roots ($\text{mg m}^{-2} \text{s}^{-1}$) which is given by

$$R_{\text{soil}} = a L_t e^{(b T_{s,s})} \quad (16)$$

where $T_{s,s}$ is the soil surface temperature ($^{\circ}$ C), L_t the total leaf area index (m^2 leaf m^{-2} ground) and a and b are constants defined below. Norman *et al.* (1992) compared several formulae of soil surface CO_2 fluxes which employed a combination of soil temperature, soil moisture and leaf area index. Preliminary tests with our dataset revealed that incorporating the effect of soil moisture in Eqn 16 did not improve the predictions and hence it was omitted.

With F_c obtained from Eqn 15, the CO_2 concentration at canopy source height, C_0 (mg m^{-3}) can be calculated using

$$C_0 = C_r - 1.4 r_{a,s} F_c \quad (17)$$

where the factor 1.4 accounts for the difference between boundary layer resistances for CO_2 and H_2O . Here, C_r is the atmospheric CO_2 concentration (mg m^{-3}).

Finally, the surface level values of C are given by

$$C_{s,i} = C_0 - 1.4 \mu_{c,i} \alpha_i L_i^* P_{n,i}. \quad (18)$$

These values, and values of $T_{s,i}$ and $D_{s,i}$, are required in the stomatal conductance-photosynthesis parameterisation described in Appendix 1.

The set of Eqns 1-18 and the model in Appendix 1 are solved for r_i by iteration.

2.2. Growth model

The extended SVAT employs a module describing plant growth, which allows values of L_i (and L_i^*), as used above, to be calculated from net CO_2 uptake. The plant growth model used in this report is based on the crop growth simulator SUCROS (Van Keulen *et al.* 1982; Spitters *et al.* 1989; Goudriaan *et al.* 1992).

Increase in biomass, W , and leaf area index, L , are calculated separately for the bushes, herbs and grasses. The initial leaf biomass for the bushes is taken from measurements, whereas the values for the herbs and grasses are derived from

$$W_{lv,0} = L_0 / s \quad (19)$$

with s the specific leaf area of new leaves (ha kg^{-1} leaf), $W_{lv,0}$ initial biomass of the leaves (dry matter) in kg ha^{-1} , and L_0 initial leaf area index ($\text{m}^2 \text{m}^{-2}$). The values of s , $W_{lv,0}$ and L_0 for each of the components are given in Table 1, together with the initial values of stem and root biomass, $W_{st,0}$ and $W_{r,0}$.

Daily total carbohydrate production, C ($\text{kg CH}_2\text{O ha}^{-1} \text{d}^{-1}$), is found from

$$C = \frac{M_{\text{CH}_2\text{O}}}{M_{\text{CO}_2}} \frac{\sum_{t=0h}^{t=24h} P_n}{100} \quad (20)$$

with P_n the net photosynthesis in $\text{mg CO}_2 \text{m}^{-2} \text{s}^{-1}$ and $M_{\text{CH}_2\text{O}}$ and M_{CO_2} the molar weights of carbohydrate (30 g mol^{-1}) and carbon dioxide (44 g mol^{-1}), respectively. The multiplication by $30/44$ is necessary because for each kg of CO_2 absorbed only $30/44 \text{ kg}$ carbohydrates is formed.

Part of the carbohydrates is respired to provide energy for maintaining the existing biostructures. The total maintenance respiration, R_m ($\text{kg CH}_2\text{O ha}^{-1} \text{d}^{-1}$) is given by:

$$R_m = f(T) F_r (m_{lv} W_{lv} + m_{st} W_{st} + m_r W_r) \quad (21)$$

with m_{lv} , m_{st} and m_r the maintenance coefficients ($\text{kg CH}_2\text{O kg}^{-1}$ dry matter d^{-1}), for a species-dependent reference temperature, of the various plant organs (leaves, stems and roots). Higher temperatures accelerate the turnover rates in plant tissue and hence increase the cost of maintenance, which is simulated by multiplication with the temperature-dependent function, $f(T)$:

$$f(T) = 2^{(T_a - T_{ref})/10} \quad (22)$$

where T_a is the air temperature and T_{ref} a reference temperature set to $25 \text{ }^\circ\text{C}$.

F_r is a reduction factor related to plant ageing

$$F_r = W_{lv} / (W_{lv} + W_{st} + W_{rt}) \quad (23)$$

which assumes that respiration is proportional to the fraction of the accumulated leaf weight that is still green. The reduction factor is also applied to maintenance respiration of the other organs as it is assumed that dying of stem tissue and roots proceeds simultaneously to dying of leaves (Goudriaan *et al.* 1992).

The primary assimilates in excess of the maintenance costs are available for conversion into vegetative plant material. Partitioning over the various organs is described by fixed distribution factors. The partitioning occurs in two steps: dry matter is first partitioned between shoots, f_{sh} , and roots, f_{rt} . That is:

$$f_{rt} = 1 - f_{sh} \quad (24a)$$

followed by the distribution of the shoot fraction among leaves, f_{lv} , and stems, f_{st} :

$$f_{st} = 1 - f_{lv} \quad (24b)$$

The factors f_{sh} and f_{lv} for the three surface components are given in Table 1.

The assimilate requirement for dry matter production, A , ($\text{kg CH}_2\text{O kg}^{-1} \text{ d.m.}$) is calculated as the weighted mean of the requirements for the different plant organs:

$$A = f_{sh}(A_{lv}f_{lv} + A_{st}f_{st}) + A_{rt}f_{rt} \quad (25)$$

where A_{lv} , A_{st} and A_{rt} equal 1.463, 1.513 and 1.444 $\text{kg CH}_2\text{O kg}^{-1} \text{ d.m.}$, respectively.

The gross growth rate of plant dry matter can then be described with

$$r = (C - R_m) / A \quad (26)$$

and the growth of plant organs with

$$G_{rt} = f_{rt}r \quad (27a)$$

$$G_{lv} = f_{lv}f_{sh}r \quad (27b)$$

$$G_{st} = f_{st}f_{sh}r \quad (27c)$$

The increase in dry matter (biomass) is found from

$$W_j(\text{day}) = W_j(\text{day} - 1) + G_j \quad \text{with } j = \text{rt, lv or st.} \quad (28)$$

and, finally, the increase in leaf area index, L , from

$$L(\text{day}) = L(\text{day} - 1) + sG_{lv} \quad (29)$$

with day the day number.

2.3. Soil heat and moisture transport

A second extension of the original, calibrated SVAT (as presented in Section 2.1) was the incorporation of a soil physical model to obtain independent estimates of soil heat flux, G , and soil moisture content, θ , (to be used for updating root-weighted volumetric soil moisture content, θ_r , see Eqn A11, and making r_s , a function of θ instead of day number).

The description of heat and water transfer in the soil was taken mainly from the SALSA (Soil-Atmosphere Linking Simulation Algorithm) simulation model (Ten Berge 1990). This model was designed to describe the interaction between a bare soil and the atmosphere and therefore features a simple Atmospheric Boundary Layer model although, alternatively, it can be run with prescribed courses of temperature, humidity and wind speed at reference (screen) height.

In this report, only the SALSA soil formulation is used and it is coupled to the SVAT described in Section 2.1. Furthermore, a simple description of soil moisture extraction by the roots (i.e. via transpiration) was incorporated. For brevity, only the main equations and concepts of the model will be summarised.

Soil heat flux

In principle, there are four soil heat fluxes that need to be modelled, G_s , G_h , G_g and G_b . For the equations in Section 2.1 *measured* values of understory and bush soil heat flux were available. The understory fluxes were used to represent G_s , because of the relative bareness of the plot. Furthermore, it was assumed that $G_g = G_h = 0.5G_s$, (see Section 3.2). Ideally, the number of components (currently four) could be extended to facilitate representation of soil below the bushes, herbs and grasses. Knowing the leaf area index, the amount of radiation received by this shaded soil could be calculated and hence its energy partitioning, surface temperature and finally soil heat flux. For simplicity, however, only G_s , which is the largest flux, is calculated in the extended SVAT and it will again be assumed that $G_g = G_h = 0.5G_s$. In this case, G_b will be calculated as a fixed percentage of bush net radiation, $R_{n,b}$ ($G_b = 0.07R_{n,b}$).

To calculate G_s , the soil profile is considered as layers each of thickness $TCM(i)$ in m, which for the savannah are given in Table 2. The distance between the middle of a layer and the next (lower) layer, $\Delta z(i)$, is found from

$$\Delta z(i) = 0.5(TCM(i) + TCM(i-1)) \quad (30)$$

while $\Delta z(1)$ is $0.5TCM(1)$.

The soil heat flux in SALSA consists of two terms: soil heat flux caused by conduction mechanisms and soil heat flux stemming from vaporisation. Hence, the soil heat flux going into the bare soil surface, G_s , is found from

$$G_s = -K_T(1) \frac{(T_{s,s} - T(1))}{\Delta z(1)} + \lambda E_s \quad (31)$$

where $K_T(1)$ is the thermal conductivity ($\text{W m}^{-1} \text{K}^{-1}$) of layer 1, $T_{s,s}$ is the soil surface temperature and $T(1)$ is the soil temperature in the middle of the first soil layer. $-\lambda E_s$ is the soil evaporation (W m^{-2} ground area) as calculated by the SVAT. The soil heat flux through the lower layers, $i = 2, N$ is given by

$$F_H(i) = -\overline{K_T(i)} \frac{(T(i) - T(i-1))}{\Delta z(i)} + F_v(i) \quad (32)$$

where $\overline{K_T(i)}$ is the mean thermal conductivity ($\text{W m}^{-1} \text{K}^{-1}$), $T(i)$ the soil temperature and $F_v(i)$ the soil latent heat flux (W m^{-2}) for layer i .

The weighted mean thermal conductivity for layer 1 is $K_T(1)$, whereas for the other layers

$$\overline{K_T(i)} = (K_T(i-1)TCM(i-1) + K_T(i)TCM(i)) / (TCM(i-1) + TCM(i)). \quad (33)$$

$K_T(i) = \frac{\rho_d^b(i)}{\rho_{d,stan}^b} f(\theta(i))$, where $\rho_d^b(i)$ is the dry bulk density of layer i and $\rho_{d,stan}^b$ is the standard dry bulk density for a certain soil type. $f(\theta(i))$ is a power function of water content, θ , specific for this Sahelian soil ($r^2 = 0.88$):

$$f(\theta(i)) = 3.57\theta(i)^{0.368}. \quad (34)$$

Finally, the rate of change in soil temperature can be calculated with

$$\frac{\partial T(i)}{\partial t} = \frac{F_H(i+1) - F_H(i)}{TCM(i)C_h(i)} \quad (35)$$

where C_h is the volumetric soil heat capacity ($\text{J m}^{-3} \text{K}^{-1}$):

$$C_h(i) = \phi_c(i)C_{h,c} + \phi_q(i)C_{h,q} + \phi_o(i)C_{h,o} + \theta(i)C_{h,w} \quad (36)$$

with ϕ_c , ϕ_q , and ϕ_o ($\text{m}^3 \text{m}^{-3}$) the volume fractions of clay, quartz and organic matter respectively. $C_{h,c}$, $C_{h,q}$, $C_{h,o}$ and $C_{h,w}$ are the volumetric heat capacities of clay, quartz, organic matter and water, respectively, which have values of 2.4, 2.1, 2.5 and 4.2 $\text{MJ m}^{-3} \text{K}^{-1}$.

The flux of water vapour for layers $i=2, N$ is found from

$$F_v(i) = \beta \overline{D(i)} \frac{\rho_v(i) - \rho_v(i-1)}{\Delta z(i)} \quad (37)$$

where $\overline{D(i)}$ is an average vapour diffusivity ($\text{m}^2 \text{s}^{-1}$) for layer i , ρ_v is the vapour density in the soil air (kg m^{-3}) and β is the vapour diffusion enhancement factor (set to 2.0, see Ten Berge 1990).

$\overline{D(i)}$ is defined by $\sqrt{D_o(i)D_o(i-1)}$, where D_a is the water vapour diffusivity in free air ($\text{m}^2 \text{s}^{-1}$). D_a is calculated with $D_o(i) = D_0 \left((T(i) + T_0) / T_0 \right)^{1.75}$ with D_0 ($2.29 \cdot 10^{-5}$) being the vapour diffusivity at 10°C and $T_0 = 273.15 \text{ K}$.

The vapour densities are given by

$$\rho_v(i) = h(i)\rho_{vs}(i) \quad (38)$$

where h is the relative humidity of the soil air (ranging from 0-1.0) and ρ_{vs} the saturated vapour density in soil air (kg m^{-3}). ρ_{vs} is parameterised as an exponential function of soil temperature, whereas h is a function of soil moisture, θ ($\text{m}^3 \text{m}^{-3}$), using a simplified adsorption isotherm (see Ten Berge 1990):

$$h = \frac{\theta \rho_w}{f_c \rho_c} \frac{0.8}{A} \quad \text{for } 0 < \theta < \theta_{30} \quad (39a)$$

$$h = 0.8 + 0.2 \left(\frac{\theta - \theta_{30}}{\theta_{1.5} - \theta_{30}} \right) \quad \text{for } \theta_{30} < \theta < \theta_{1.5} \quad (39b)$$

$$h = 1.0 \quad \theta > \theta_{1.5} \quad (39c)$$

with ρ_w the density of soil water (1000 kg m^{-3}), f_c the volume fraction of clay, ρ_c the density of clay (2650 kg m^{-3}) and A ($0.01 \text{ kg water kg}^{-1} \text{ clay}$ for kaolinite clay, typical for leached tropical soils) the gravimetric moisture content at $h = 0.8$. θ_{30} is the corresponding volumetric water content at -30 MPa (equivalent to $h = 0.8$), which is given by $1 / \frac{A}{f_c \rho_c}$.

$\theta_{1.5}$ is the wilting point (pressure 1.5 MPa , $h \approx 0.99$), given by

$$\theta_{1.5} = (\theta_s - \theta_r) \left((15^5 \alpha)^n + 1 \right)^{-1/n} \quad (40)$$

which is another point to define the adsorption isotherm. θ_s and θ_r are the saturated and reference soil moisture content, while α (Pa^{-1}) and n (-) are Van Genuchten hydraulic parameters (see Table 3).

The liquid soil water flux, F_l , is calculated using the concept of matrix flux potential (Raats 1970) so that for $i = 2, N$

$$F_l(i) = (\Phi(i) - \Phi(i-1)) / \Delta z(i) + F_g(i) \quad (41)$$

where $\Phi(i)$ is the matrix flux potential ($\text{kg m}^{-1} \text{s}^{-1}$) and F_g is the liquid soil water flux due to gravity ($\text{kg m}^{-2} \text{s}^{-1}$). The matrix flux potential for $i = 1, N$ is calculated from

$$\Phi(i) = S \frac{-M_a(1 - \theta(i) / \theta_m)}{(1 - \theta(i) / \theta_m) + M_b} \quad (42)$$

with M_a and M_b soil dependent coefficients and θ_m the reference moisture content in the matrix flux potential. Φ is multiplied by a scale factor, S , to allow for easy changes in hydraulic scale, simultaneously affecting moisture characteristic, conductivity and matrix flux potential. For the top layer, $F_1(1)$ is the maximum of infiltrated rainfall over a half hour period, P ($\text{kg m}^{-2} \text{s}^{-1}$), and $\Phi(1) / \Delta z(1) + F_g(1)$.

F_g is given by $F_g(i) = \rho_s g \overline{K(i)}$, with g the gravitational acceleration (m s^{-2}) and $\overline{K(i)}$ the average hydraulic conductivity defined by $\overline{K(i)} = S^2 \sqrt{K(i-1)K(i)}$ ($\text{kg m}^{-1} \text{Pa}^{-1} \text{s}^{-1}$), for $i=2, N$, while $\overline{K(1)} = K(1)$. For $\theta(i) \geq \theta_r$, $K(i)$ is calculated from

$$K(i) = K_s \Xi(i)^{0.5} \left(1 - \left(1 - \Xi(i)^{1/m} \right)^m \right)^2 \quad (43)$$

where K_s is the saturated hydraulic conductivity ($\text{kg m}^{-1} \text{Pa}^{-1} \text{s}^{-1}$). For $\theta(i) < \theta_r$, $K(i) = 0.0$. In Eqn 43

$$\Xi(i) = \frac{\theta(i) - \theta_r}{\theta_s - \theta_r} \quad \text{and } m = 1 - 1/n. \quad (44)$$

Finally, the total soil water flux is found from

$$F_w(i) = F_1(i) + F_v(i) \quad (45)$$

from which the rate of change in soil moisture can be calculated using

$$\frac{\delta\theta(i)}{\delta t} = \frac{(F_w(i+1) - F_w(i))}{\rho_s TCM(i)} + \frac{R_{ex}(i)}{\rho_s TCM(i)} \quad (46)$$

where $R_{ex}(i)$ is the root extraction resulting from transpiration from that layer. The latter term on the RHS of Eqn (46) was not included in the original SALSA model, but has been added here to enable changes in soil moisture caused by transpiration and not just by evaporation from the soil.

$R_{ex}(i)$ was obtained from root density measurements of the bushes and the herb layer. The absolute root density for the bushes, R_b and the undergrowth, R_u at a certain depth below the surface, $z(i)$, is given by

$$R_b = 0.1893 \exp(-1.82z(i)) \quad (47a)$$

$$R_u = 0.5062 \exp(-4.98z(i)) \quad (47b)$$

where $z(i)$ is incremented from 0 to 2.0 m (depth of soil profile) with steps of 0.10 m. The cumulative root density, ΣR_b and ΣR_u ($0 < \Sigma R \leq 1.0$), i.e. the fraction of roots between the soil surface and level $z(i)$, can be calculated, and the root total extraction, $R_{ex}(i)$, found using

$$R_{ex}(i) = (\Sigma R_b(i) - \Sigma R_b(i-1)) \lambda E_b + (\Sigma R_u(i) - \Sigma R_u(i-1)) \lambda E_u \quad (48)$$

where λE_b and $\lambda E_u (= \lambda E_h + \lambda E_g)$ are the transpiration of the bushes and understorey (in W m^{-2} ground area), respectively.

Finally, soil moisture and soil temperature are updated with

$$\theta(t,i) = \theta(t-1,i) + \Delta t \delta \theta / \delta x \quad (49a)$$

$$T(t,i) = T(t-1,i) + \Delta t \delta T / \delta x \quad (49b)$$

where $\Delta t = 1800$ s, and $\theta(t-1,i)$ and $T(t-1,i)$ are the soil moisture content and temperature at the previous timestep. $\theta(0,i)$ and $T(0,i)$ are given in Table 2.

3. MATERIAL AND METHODS

3.1. Description of field site and conditions

Most data used in this study were collected by the Department of Meteorology, Wageningen Agricultural University (WAUMET), the Netherlands, over a sparse West-African savannah consisting of *Guiera senegalensis* (C_3 metabolic pathway) bushes (20% areal coverage), with a mixed understorey of grasses and herbs (50%) and bare soil (30%). The dominant herb was *Mitracarpus scaber* (C_3 metabolism), while the grass layer was represented by the dominant species *Digitaria guyana* (C_4 metabolism). The soil type can be described as sandy with 93% sand, 3% silt, and 4% clay (M. Soet, personal communication, 1998). Measurements took place in the HAPEX-Sahel campaign (Goutorbe *et al.* 1994) during August-October 1992 within the Central West Supersite, CWS, (see Kabat *et al.* 1996; Gash *et al.* 1997) in the vicinity of Niamey, Niger.

Only data obtained between days 251 and 283 (6 September - 9 October 1992) were used in this report. During the first two weeks of this period conditions were generally cloudy with rainfall occurring during the early morning of day 251 (20 mm), the afternoon of day 254 (8 mm), the morning of day 256 (12 mm), the evening of day 258 (8 mm), and during the early morning (8mm) and afternoon (2 mm) of day 259. The last rainfall occurred during the early morning of day 264 (0.5 mm). Thereafter, cloud cover rapidly decreased and virtually cloudless skies dominated during the remainder of the experimental period.

The total undergrowth reached a maximum leaf area index, L_u , of 1.0 near the end of the measurement campaign. Bush leaf area index, L_b , increased from zero at the start of the rains in June to about 0.35 at the end of October (Hanan & Prince 1997). After 1 October there was leaf yellowing and signs of senescence which were accounted for in the model by decreasing L of all three species by $0.01 \text{ m}^2 \text{ m}^{-2}$ per day. More details of the experimental site are given in Verhoef (1995), Verhoef *et al.* (1996a) and Kabat *et al.* (1996).

3.2. Environmental driving and verification data

Micrometeorological data

Rainfall was sampled using a classical tipping bucket gauge, with a 400-cm^2 collector. Each tipping, corresponding to 0.5 mm of rainfall, was recorded to the second, which meant intensities of up to 1800 mm h^{-1} were measurable. This gauge was located in close vicinity of the WAUMET site (distance $\approx 50 \text{ m}$) and was part of a 100 gauge network, which operated permanently between mid-April and the end of November of each year between 1990 and 1993 (see Lebel *et al.* 1997). Rainfall was accumulated into half-hourly sums. For the climate change sensitivity model runs, these rainstorms were converted into units of $\text{kg m}^{-2} \text{ s}^{-1}$ and assumed to occur instantaneously at the beginning of each half-hour interval. Only 70% of each rainstorm was assumed to infiltrate into the soil because of interception and local runoff. This is a representative value for Sahelian soils (see Stroosnijder 1982; Soet *et al.* 1993). For the calibration

run, which was made with the SVAT described in Section 2.1, rainfall input data were not required.

The driving variables, D_r and T_r at $z = 4.5$ m were measured using a psychrometer, while u_r was measured with a cup anemometer. Both instruments were manufactured at WAUMET. Values for atmospheric CO_2 concentration, C_r , were obtained with an infrared gas analyser (Model LI-6262, LI-COR Inc., Lincoln, NE, USA) with the inlet located at a height of 5.0 m. R_{sol} was measured with a solarimeter (Type CM5, Kipp and Zn, Delft, the Netherlands) at a height of 10 m, while $R_{\text{t},\text{a}}$ was calculated from $R_{\text{t},\text{a}} = \varepsilon_a \sigma T_r^4$, employing Brutsaert's (1975) equation, using vapour pressure and air temperature, to find atmospheric emissivity, ε_a .

Soil heat flux under the bushes, G_b , was estimated as the average of the output from nine thermopile flux plates (TNO, Delft, the Netherlands) installed under a shrub at an average depth of 0.04 m. Shallow soil temperature measurements were used to correct G_b for the heat storage in the soil layer overlying the plates. G_h , G_s and G_t were derived from an estimate obtained from the calorimetric method (G_{cal}) using a soil temperature profile at a sparsely vegetated plot, measured with horizontally inserted PT-100 resistance thermometers, and corresponding estimates of soil heat capacity (see Verhoef *et al.* 1996b). For the calibration run, it was assumed that $G_s = G_{\text{cal}}$ and $G_h = G_t = 0.5G_{\text{cal}}$, whereas in the extended SVAT version G_s (and $G_h = G_t$ from $0.5G_s$) was calculated with the soil model described in Section 2.3.

For model verification, the evaporative, sensible heat and net CO_2 fluxes were measured at a height of 5m with the eddy covariance technique using a three-axis sonic anemometer (Solent A1012R2, Gill instruments Ltd., Lymington, Hampshire, UK) and the differential closed-path infra-red gas analyser (see Verhoef 1995; Moncrieff *et al.* 1997). Due to instrument problems, no atmospheric flux data were available for days 257-260, day 271 and the morning of day 272, day 278 and during the middle of day 280. Separate values of soil respiration were not measured and it is explained below how estimates of this flux were obtained.

Total net radiation was measured at a height of 10 m using a net radiometer (type Middleton, Funk, Germany). Values of the surface temperature were obtained using infra-red thermometers, IRTs, (type KT15, Heimann, Wiesbaden, Germany). One IRT was installed at a height of 1.60 m and was pointed downwards (90° orientation) above the understorey between the shrubs, causing the instrument to 'see' between the upright blades of grass. Its readings were therefore used to represent the surface temperatures of bare soil, $T_{\text{s},\text{a}}$. The other IRT was pointed horizontally at the north-facing side of a bush and used to verify predictions of $T_{\text{s},\text{b}}$ made by the model. Surface temperatures of the herbs and the grasses were not measured.

Soil moisture and soil temperature data

Profiles of volumetric soil water content ($\text{m}^3 \text{m}^{-3}$) were obtained every other day using neutron probes (CPN Hydroprobe, Model 503) and Time Domain Reflectometry (TDR). Four neutron access tubes were located close (within ≈ 150 m) to the WAUMET site (tubes 23, 24, 25 and 29), which were all installed under a relatively sparse herbaceous understorey. The plots were either flat (local slope 0-1 a 2%) or slightly sloping (1 a 2% - 3%). All plots were located within a radius of 2 m from a bush. Neutron probe measurements were made at depths of approximately 0.15, 0.25, 0.35, 0.45, 0.6, 0.75,

0.95, 1.15, 1.35, 1.55 and 1.70 m. The procedure involved one 16 s count time reading per depth layer (Cuenca *et al.* 1997). The access tube no. 24 (\approx 50 m away from the WAUMET site) was surrounded by TDR-probes in triplo at depths of 0.05, 0.10 (horizontal), 0.2-0.3 and 0.4-0.5 (vertical) m.

For verification of the soil moisture predictions of the model, we used the TDR measurements (average of probes at 0.10 and 0.2-0.3 m) for the first soil layer (0-0.3 m, see Table 2). This was done because of the relative inaccuracy of neutron probes close to the surface. The θ -estimates for the other layers were compared with the neutron probe data of tube 23 (\approx 75 m away from the WAUMET site, in close proximity to the rain gauge). Because of the thickness of the layers chosen in the model configuration (see Table 2) the data at (exact) depths of 0.41, 0.81, 1.21 and 1.76 m were used to calibrate and verify the soil moisture predictions.

Soil temperatures have been measured with PT-100 resistance thermometers horizontally inserted at several depths at two plots, located approximately 5 m apart. The resistance elements had a diameter of about 3 mm. Both temperature profiles were located beneath the directly exposed understorey. One of the plots was sparsely vegetated, whereas the other plot exhibited more vegetation (grass and herbs) than average. Each temperature array consisted of five thermometers installed at depths of 0.03, 0.05, 0.10, 0.25 and 0.50 m. For verification of the soil temperatures in the centre of compartment 1 and 2 (0.15 and 0.45 m depth, respectively), we used the average of the thermometers located at depth 0.10 and 0.25 m and the deepest thermometer, both installed under the sparsely vegetated plot.

To measure thermal conductivity, thermal conductivity probes, developed by WAUMET, were placed in between the temperature sensors, at depths of 0.015, 0.04, 0.075, and 0.15 m. They were connected to a portable data logger several times per day (three times during the wet period, one or two times during the dry period) so they could be read. The values obtained at 0.15 m under the relatively bare plot, in combination with the average of the TDR measurements at 0.10 and 0.2-0.3 m were used to derive the K_T - θ dependency employed in the model (see Eqn 34).

Vegetation data

Leaf stomatal conductance data, $g_{l,i} = 1/r_{l,i}$, as measured with a porometer, were obtained for the three main plant types (Verhoef 1997; Hanan & Prince 1997), which allowed for calculation of the eight model parameters describing $P_{n,i}$ and $r_{l,i}$, using a non-linear least squares optimization as will be explained later. Measurements of *Mitracarpus scaber* leaf conductance, representing $g_{l,h}$, were multiplied by 0.75, as measurements of $g_{l,h}$ were suspected to be too high (see Verhoef 1997).

Leaf area index, L (m^2 leaf m^{-2} soil), and biomass ($kg\ ha^{-1}$) estimates at the CWS were obtained by harvest methods. *Guiera senegalensis* leaf and new wood dry biomass and herb layer dry biomass were estimated at intervals throughout the growing period. The sampling method for *Guiera* involved destructive harvesting of 12-30 bushes at each date, separation of leaf and new wood material and determination of dry weight. Allometric relationships were derived between bush volume and biomass for each sampling date. Area weighted estimates were obtained using the known distributions of bush dimensions and bush density on the site. Estimating the dry biomass of the herb layer involved the stratification of the total herb layer into classes of increasing biomass. This was done at 1

m intervals on 2-3 transects totalling 400-500 m in length. Destructive harvesting of 12-20 0.5 m² quadrats gave an estimate of dry mass for each class. Area weighted estimates were obtained using the known frequency of each class obtained from the transects (Hanan *et al.* 1997).

Because biomass estimates are subject to sampling error, day-number dependent growth curves fitted to the data were used (HAPEX-Sahel database, N. Hanan).

$$B_l = a_l \exp^{-\exp(-b_l(DAY-c_l))} \quad (50a)$$

$$B_w = a_w \exp^{-\exp(-b_w(DAY-c_w))} \quad (50b)$$

$$B_h = a_h (1.0 + \exp(-b_h(DAY - c_h)))^{-1} \quad (50c)$$

where B_l , B_w and B_h are the *Guiera* leaf biomass, *Guiera* new wood biomass, and the herb layer leaf biomass in kg ha⁻¹, respectively. The constants are $a_l = 357.4$, $a_w = 179.9$, $a_h = 1324.5$, $b_l = -0.0392$, $b_w = 0.0012$, $b_h = 0.0872$, $c_l = 200.045$, $c_w = 293.996$, $c_h = 258.426$.

Leaf area indices were estimated using specific leaf area (leaf area/leaf mass) relationships determined for each of the major species or, for the mixed-species herb layer, using canopy averaged values. For more information on vegetation sampling methods see Hanan *et al.* (1997).

3.3. Model parameters

Vegetation

The albedos and surface emissivities used in Eqn 10 were given the following values: $a_b = a_h = a_g = 0.20$, $a_s = 0.25$, $\epsilon_b = \epsilon_h = \epsilon_g = 0.98$, $\epsilon_s = 0.93$. The leaf widths of the bushes, herbs and grasses, l_i , needed in Eqn 4, were 0.02, 0.05 and 0.005 m, respectively. The roughness lengths, $z_{om,i}$, for the bushes and understorey, as required in Eqns 3-5 were taken as 10% of their respective heights, which were set to 2.3 and 0.5 m, respectively. Displacement height, d_i , was calculated as 75% of the upperstorey and understorey height. The effective displacement and roughness length for the total surface were obtained from the model as described in Verhoef *et al.* (1997), giving the values $z_{om} = 0.25$ m and $d = 1.5$ m. The decay coefficient n was assumed to be 2.5, which is a value used in many SVATs (see Shuttleworth & Wallace 1985, for example).

The coverage fractions were $\alpha_b = 0.2$, $\alpha_h = \alpha_g = 0.5$ and $\alpha_s = 0.3$. For all three vegetation types μ is set to a standard value of 1.0. For the calibration runs, values for L_i^* and L_i and the values of root-weighted volumetric soil moisture content, θ_i (see Eqn A11) were obtained from N. Hanan (personal communication, 1994). For the extended model runs these values were found from the descriptions of growth and soil moisture distribution given in Sections 2.2 and 2.3. The constant c in Eqn A10, related to the soil moisture status, equals -1498 and -2313 m for *Mitracarpus* and *Digitaria*, respectively (see Hanan & Prince, 1997). The soil moisture-related multiplication factor, f_θ (see Eqn A10), was set to 1.0 for the bushes.

Table 1 gives the parameters required in the growth model (Section 2.2). L_0 estimates for *Mitracarpus* and *Digitaria* were derived from measurements of total

undergrowth leaf area index and estimates of relative contribution of herbs and grasses to the undergrowth L by N. Hanan (personal communication, 1994). Values of s were taken from Hanan *et al.* (1997). *Guiera* root production was not measured in the field. To find $W_{r,0}$ for this species it was assumed that total root production was equal to total above-ground production. $W_{r,0}$ for the two undergrowth species was estimated as $2 W_{lv,0}$. The shoot and leaf fraction were not measured and had to be derived from the literature (Breman & Kessler 1995).

Table 1. Plant parameters used in the growth model. Values are based on measurements unless followed by *, which indicates they are estimated.

	<i>Guiera</i>	<i>Mitracarpus</i>	<i>Digitaria</i>
L_0 (day 251)	0.286	0.272*	0.129*
$W_{lv,0}$ (day 251)	312	266 (L_0/s)*	258 (L_0/s)*
$W_{st,0}$ (day 251)	34.5	80*	65*
$W_{r,0}$ (day 251)	350*	532 ($2 W_{lv,0}$)*	516 ($2 W_{lv,0}$)*
s	0.000916	0.001024	0.0005
f_{sh}	0.4*	0.3*	0.5*
f_{lv}	0.6*	0.7*	0.7*

Soil

Table 2 gives the thickness of the 5 soil layers, as required in Eqn 30, among others, and the initial model estimates of soil moisture and soil temperature.

Table 2. Thickness of soil compartments and initial (Day 251, 0.25 h) profiles of soil moisture and soil temperature.

i	$\Delta z(i)$ [m]	$\theta(0,i)$ [$m^3 m^{-3}$]	$T(0,i)$ [$^{\circ}C$]
1	0.3	0.10	29.1
2	0.3	0.11	33.6
3	0.4	0.11	34.0
4	0.5	0.11	35.0
5	0.5	0.11	35.0

Table 3 shows the various model parameters used in the soil algorithm. M_s , M_b and n were obtained from Stroosnijder (1982) which represent a Sahelian sandy soil. α , K_s , θ_i and θ_s were derived from the multistep outflow method, which is a laboratory method involving fitting of a one-dimensional unsaturated flow model, which describes soil hydraulic properties using the analytical Mualem-Van Genuchten functions, on a measured timeseries of soil core outflow data (see Soet *et al.* 1993). This method also provided a value for n (2.38), but preliminary testing indicated that a lower value suited the data better, and hence the value of 1.4 as given by Stroosnijder (1982) was adopted.

Dry bulk densities ρ_d^b were taken as 1530, 1400, 1350, 1300 and 1300 for layers 1 to 5 (see Verhoef *et al.* 1996b).

Table 3. Model parameters used in the soil algorithm.

Parameter/variable	Value	Units
Number of soil compartments, N	5	-
<i>Hydraulic soil properties</i>		
Saturated soil moisture content, θ_s	0.36	$\text{m}^3 \text{m}^{-3}$
Residual soil moisture content, θ_r	0.01	$\text{m}^3 \text{m}^{-3}$
Reference soil moisture content in matrix flux potential, θ_m	0.25	$\text{m}^3 \text{m}^{-3}$
Parameter in matrix flux potential function, M_a	0.000471	$\text{kg m}^{-1} \text{s}^{-1}$
Parameter in matrix flux potential function, M_b	0.046	-
Saturated hydraulic conductivity, K_s	0.0000021	$\text{kg m}^{-1} \text{Pa}^{-1} \text{s}^{-1}$
Van Genuchten parameter, α	0.000356	Pa^{-1}
Van Genuchten parameter, n	1.4	-
Scale factor, S	2.0	-
<i>Soil composition</i>		
Volume fraction clay, ϕ_c	0.04	$\text{m}^3 \text{m}^{-3}$
Volume fraction quartz, ϕ_q	0.45	$\text{m}^3 \text{m}^{-3}$
Volume fraction organic matter, ϕ_o	0.01	$\text{m}^3 \text{m}^{-3}$
Porosity, ϕ	0.50	$\text{m}^3 \text{m}^{-3}$
Standard dry bulk density $\rho_{d,\text{stan}}^b$ (sandy soils)	1500	kg m^{-3}

3.4. Optimisation of photosynthesis-leaf conductance model

Least-squares estimates of the eight parameters, $g_m(@25)$, $P_{m,\text{max}}(@25)$, $g_m(T_1)$, $g_m(T_2)$, $P_{m,\text{max}}(T_1)$, $P_{m,\text{max}}(T_2)$, $D_{s,\text{max}}$ and f_0 , required for the description of leaf stomatal resistance of *Guiera senegalensis*, *Mitracarpus scaber* and *Digitaria guyana* were obtained using a nonlinear regression procedure involving Eqns 1-18. This procedure was executed three times to find the stomatal resistance parameters for the bushes, herbs and grasses, respectively, using an input file containing 74 simultaneous half-hourly observations of $g_{l,b}$, $g_{l,h}$ and $g_{l,g}$, together with the required atmospheric driving variables R_{soil} , T_r , D_r , C_r , u_r , and root-weighted volumetric soil moisture content, θ_r . While finding the parameter estimates for the bushes, for example, measured values of $g_{l,h}$ and $g_{l,g}$ were used to calculate λE_h , λE_g etc. Measured values of F_c were used to find C_0 from Eqn 17, so estimates of $P_{n,i}$ and R_{soil} (see Eqn 15) were not required during this optimisation.

3.5. Parameterisation of soil respiration

Having obtained the model parameters from the fitting procedure described above, the model was run with all the half-hour values available between days 251 and 284 as input. This was done to determine the values of soil respiration, because, as mentioned above, direct measurements of this flux were not available. The values for R_{soil} were derived from Eqn 15, using measured values of F_c and model estimates of $P_{n,b}$, $P_{n,h}$, and $P_{n,g}$. In this way 960 half-hourly values of R_{soil} were determined, representing both daytime and nighttime conditions. Consecutively, values for the parameters a and b in Eqn 16 were then optimised using these 960 values of soil respiration, together with values of total L and predicted soil surface temperature ($T_{s,s}$).

The calibrated Eqn 16 describing soil respiration, allowed us to perform a final run yielding estimates of F_c , the energy balance and surface temperatures. The model predictions of this calibrated run will be verified below.

3.6. Water use efficiency

The component predictions of $P_{n,i}$ and λE_i can be used to calculate water use efficiency, WUE , an important parameter in agricultural studies. WUE can be defined as the ratio between photosynthesis and transpiration (e.g. Jones 1983; Baldocchi *et al.* 1985). Here, we modelled the dimensionless WUE as:

$$WUE_i = \lambda \cdot 10^{-6} (\alpha_i L_i^* P_{n,i} / \alpha_i \lambda E_i) \quad (51)$$

Because indices of photosynthesis over transpiration have been reported to be sensitive to low levels of irradiance (Baldocchi *et al.* 1985), WUE will only be calculated for periods when $R_{\text{soil}} > 300 \text{ W m}^{-2}$ (see also Verhoef *et al.* 1996a).

3.7. Procedure for sensitivity analysis

To investigate the effect of a possible change in climate, a sensitivity analysis was performed with the extended SVAT using three perturbations. These were: (i) doubled concentration of atmospheric CO_2 , (ii) air temperature increased by $1.5 \text{ }^\circ\text{C}$ and (iii) both (i) and (ii) applied. The fluxes and surface temperatures predicted by the three perturbation runs were compared to the results for the reference run. For this comparison the average diurnal course of the experimental period was calculated ($n \approx 1490$ half-hourly flux estimates).

The results of the reference run (the extended model with standard input of C_i and T_i) will be verified first (Section 4.6) to ensure they are a realistic representation of the savannah ecosystem.

4. RESULTS

4.1. Least squares fitting procedure

Table 4 shows the optimised values for the parameters in the photosynthesis-leaf conductance model as found from the least squares fitting procedure for each of the three species. The coefficients of determination, r^2 , were 0.79, 0.47 and 0.74 for *Guiera*, *Mitracarpus* and *Digitaria*, respectively.

Table 4. Parameters in the photosynthesis-leaf conductance model (see Appendix 1) derived from the porometry data for *Guiera Senegalensis*, *Mitracarpus scaber* and *Digitaria*. X(@25) denotes the parameter value at 25 ° C.

<i>Guiera Senegalensis</i>	Parameter (X)	X(@25)	T_1 (°C)	T_2 (°C)
	g_m (m s ⁻¹)	0.0147	6	37
	$P_{m,max}$ (mg m ⁻² s ⁻¹)	0.70	6	37
	$D_{s,max}$ (mbar)	29.9		
	f_0 (-)	0.94		
<i>Mitracarpus scaber</i>				
	g_m (m s ⁻¹)	0.0013	3	47
	$P_{m,max}$ (mg m ⁻² s ⁻¹)	1.6	3	52
	$D_{s,max}$ (mbar)	59.1		
	f_0 (-)	0.96		
<i>Digitaria guyana</i>				
	g_m (m s ⁻¹)	0.0087	9	41
	$P_{m,max}$ (mg m ⁻² s ⁻¹)	0.75	9	43
	$D_{s,max}$ (mbar)	48.0		
	f_0 (-)	0.23		

We acknowledge that a large number of parameters (eight) is fitted simultaneously and that an equally good fit could probably be obtained with a different combination of parameters. However, the parameters presented in Table 1 are fairly realistic and compare well to parameters found in the literature (see Jacobs 1994). This is underlined by the fact that $T_{1,2}$ for $g_m \approx T_{1,2}$ for $P_{m,max}$ in all three cases. Furthermore, f_0 for the grass *Digitaria* is ≈ 0.3 , which is the value quoted for C₄ species (Jacobs 1994).

4.2. The energy balance and net CO₂ flux

The parameters in Eqn 16, describing soil respiration, were $a = 0.038$ (mg m⁻² s⁻¹) and $b = 0.047$ (°C⁻¹), $r^2 = 0.70$. With the parameterisation of R_{soil} the final calibration run was performed and its estimates of the total fluxes, R_n , λE , H and F_c are compared to their measured values in Figs. 2, 3 and 4. Each graph is divided into four subgraphs with each subgraph showing 4 to 5 days. The first subgraph from the top (a) represents several days during the wet period (day number 252-256, i.e. 8-12 September), whereas

the second one (b) depicts the results for days 265-269 (21-25 September), which are just after the final rainfall. The third graph (c) shows the comparison for days 275-279 (1-5 October), when soil moisture was rapidly diminishing, while the final graph (d) gives the results for days 280-283 (6-9 October) when the vegetation was showing signs of senescence. Each day runs from 0.00 until 24.00 hours. In Figs. 2-4 the lines give the model estimates and each dot represents a half-hourly average of flux data. Only the datapoints satisfying $|R_n - \lambda E - H - G| \leq 75 \text{ W m}^{-2}$ are shown.

Fig. 2 shows very good agreement between measured and modelled values of total net radiation, during the entire measurement campaign for both daytime and nocturnal conditions. R_n appears to decrease by about 10% from the beginning to the end of the period, falling below 600 W m^{-2} during the last few days of the campaign, mainly as a result of increasing surface temperatures as will be shown in Fig. 5.

Fig. 3 generally shows a good correspondence between measured and modelled values of λE and H . During most of the days peak values of λE are between 250 and 350 W m^{-2} . Peak values of H are more variable, but they usually range between 100 - 200 W m^{-2} . Sensible heat flux becomes negative relatively early during the day (around 1600 hours GMT), which allows evaporation to continue until about 1800 hours GMT. In Fig. 3a, the cloudy conditions are the reason of the capricious course for both the measured and modelled fluxes. Agreement between predicted and measured fluxes gets better in Fig. 3b. Fig. 3c shows that towards the end of the campaign, estimates of λE are generally slightly too high (and hence estimates of H too low), which is probably a result of L being too large, even though L has been forced to decrease after day 275. A small amount of evaporation was measured during most nights which was simulated by arbitrarily setting the leaf conductance of the three vegetation types to 0.0005 m s^{-1} .

Fig. 4 shows that the measurements of F_c exhibit a large variability, especially during the night when stable conditions occurred. Although daytime maximum values of net CO_2 flux are on the whole predicted well by the model, with predictions slightly overestimating during days 280-283, the F_c values during the late afternoon transition hours are often underestimated (see Fig. 4b). During these hours, Eqn 16 is overestimating actual soil respiration. Furthermore, nighttime CO_2 efflux seems to be overestimated by the model towards the end of the period, when soil surface temperatures were generally higher, but the vegetation was senescing and hence root respiration was expected to become lower.

4.3. Surface temperatures

Fig. 5 shows the model predictions and measurements of bush and bare soil surface temperatures. Because separate continuous measurements of $T_{s,b}$ and $T_{s,g}$ were not available, only $T_{s,b}$ and $T_{s,s}$ were considered in this graph.

Measured peak surface temperatures for the bushes roughly range between 32 °C and 40 °C. Highest values were observed towards the end of the measurement campaign, especially on day 281, when high vapour pressure deficits caused leaf conductance, and hence evaporation, for all three species to be very low (see Verhoef *et al.* 1996a). During the night, lowest temperatures were about 22 °C.

Measured soil surface temperatures were lowest on days after or during which rainfall occurred: peak values on these days were about 45 °C. At the end of the

campaign values close to 60 °C were observed. During the night $T_{s,s}$ was usually very similar to $T_{s,b}$, which is to be expected.

Correspondence between measurements and data is usually very good. However, the influence of rainfall is visible in Fig. 5a: overestimations of $T_{s,s}$ occur on days 252, 255 and 256, when soil moisture had increased after rainfall occurring during the previous night or morning. With increased soil moisture the constant value of $r_{s,s} = 1000$ as used before day 261, was clearly too high. Relating $r_{s,s}$ to soil moisture, as described in Verhoef (1995), would avoid this overestimation. The rainfall during day 254 and 255 also caused a failure of the infrared radiometer installed to measure $T_{s,s}$ during the nights of days 254 and 255.

Table 5 presents the statistics for comparison between measurements (dependent variable) and model estimates (independent variable) of the fluxes and the surface temperatures. The linear regression has been forced through the origin. In all cases the model accounted for a large percentage of the variance in the measurements. Nearly all of the variance (99%) could be explained for R_n , whereas for the predictions of λE $r^2 = 0.93$. Lowest values were found for H ($r^2 = 0.82$) and F_c ($r^2 = 0.81$). For all the variables presented in Table 5, the slope was ≤ 1.0 , meaning that the model was overestimating the flux or surface temperature. On average, the overestimation was 2, 9, 11, 18, 0 and 3% for R_n , λE , H , F_c , $T_{s,b}$ and $T_{s,s}$. No noticeable non-linearities were observed for the agreement between model and measurement.

Table 5. Statistics for comparison between model predictions and measurements of energy balance fluxes R_n , λE and H , net CO_2 flux and bush and soil surface temperatures. The slope refers to the slope of a linear regression with zero intercept between data and predictions. The number of samples varies depending on the number of occasions (half hours) of instrument failure for a certain flux or surface temperature.

Variable	Slope	r^2	Number of samples
R_n	0.98	0.99	1073
λE	0.91	0.93	945
H	0.89	0.82	954
F_c	0.82	0.81	923
$T_{s,b}$	1.00	0.87	1021
$T_{s,s}$	0.97	0.93	1027

A similar pattern was observed by Baldocchi & Harley (1995), who found that their CANOAK model explained 78% of variance in measured H and 73% of the variance in F_c , as compared to 99% and 86% for R_n and λE , respectively, for 197 samples over a deciduous forest.

4.4. Predictions of component fluxes and surface temperatures

Fig. 6 shows that the largest available energy is predicted for the bushes, which have low surface temperatures, and hence low outgoing longwave radiation, and small values of soil heat flux because soil temperatures under the shaded bushes are low. The available energy for the other three surfaces is quite similar, although Fig. 6a shows that during the wet period A_g is considerably lower. This is caused by low L_g values at the start of the period because $R_{n,h}$ and $R_{n,g}$ are multiplied by their relative share in total undergrowth L (see Eqn 10).

From Fig. 7 it is clear that the bush transpiration is largest throughout the whole period. During the wet and the early dry-out period, highest values are around 600 W m^{-2} . With L_n slowly decreasing after day 275, peak values decrease to 400 W m^{-2} . With D_r increasing towards the end, λE_b starts to show signs of midday depression (see days 279, 281 and 282). Herb transpiration has a peak value of $\approx 350 \text{ W m}^{-2}$, which diminishes to $\approx 200 \text{ W m}^{-2}$ as day number increases. The rapidly developing grasses show a dramatic increase in λE_h from about 50 W m^{-2} to peak values ranging between 150 and 200 W m^{-2} . On a diurnal scale, transpiration of the grasses appears to peak after the herbs and bushes. Finally, the bare soil evaporation, with highest values of about 100 W m^{-2} , rapidly decreases after the final rainfall, when $r_{s,}$ quickly decreases.

The variation of the component sensible heat fluxes exhibits a more complicated pattern, as illustrated in Fig. 8. During most days, sensible heat flux originating from the bare soil is clearly highest, because of the small evaporation. On average, lowest values are predicted for the herbs, with $H_h \approx 0$ or going slightly negative during the afternoon. A clearer diurnal pattern, with a midday peak, is visible during the rainy period and during days 282-283. The predictions for the grasses are always positive during the daytime. The bushes exhibit a distinct diurnal pattern: after relatively high positive values during the morning, H_b sharply drops to reach negative values of down to -200 W m^{-2} . During these hours the bushes are using energy which originates from the relatively hot grasses and bare soil, to maintain their high levels of transpiration. The values of A_i , λE_i and H_i in Figs. 6-8 have to be multiplied by α_i to obtain the evaporation on a ground area basis.

Fig. 9 depicts the course of the net CO_2 assimilation on a ground area basis ($= P_{n,i} L_i$) for the three plant species together with the soil/root respiration (depicted as $-R_{\text{soil}}$). The grasses, having the lowest values during the beginning of the period (lowest L), rapidly increase to have the highest values from day 265 onwards. During most of the time the bushes and the herbs have similar values of $P_{n,i} L_i$, but the influence of the drying atmosphere clearly starts to show during the last 5 days of the campaign, when the $P_{n,b} L_b$ becomes lower and starts to dip during the middle of the day, as was also observed for λE_b . The respiration clearly increases when the plant-soil system dries out and soil temperature increases. On a leaf area basis, the three species produce quite similar values of net photosynthesis. Peak values of *Digitaria* range between 0.8 and $1.0 \text{ mg m}^{-2} \text{ s}^{-1}$, which the highest values occurring during the wet period. Between days 251-255, *Mitracarpus* reaches maximum values of $\approx 0.8-0.9 \text{ mg m}^{-2} \text{ s}^{-1}$, but peak values decrease thereafter and lowest values ($0.6 \text{ mg m}^{-2} \text{ s}^{-1}$) are observed around day 275-280 when D_r is highest. Maximum values of net photosynthesis for *Guiera* is fairly constant over the 30-day period with peak values of around $0.8 \text{ mg m}^{-2} \text{ s}^{-1}$. The diurnal course of $P_{n,i}$ for the three species is similar, especially for the bushes and the herbs.

The course of the simulated surface temperatures for the four surface components is given in Fig. 10. As expected, and as also illustrated in Fig. 5, $T_{s,i}$ is much higher than the surface temperatures of the vegetation, whereas the herbs and the bushes have very similar values during most of the days. During sunshine hours, the grasses are usually around 3-5 °C warmer than the two other species, although these differences become less towards the end of the measurement campaign. During the night all components have a similar temperature.

4.5 Water use efficiency

Fig. 11 shows the modelled dimensionless water use efficiency of the three species as a function of their surface vapour pressure deficits, $D_{s,i}$.

For the two C_3 species, *Guiera* and *Mitracarpus*, *WUE* ranges roughly between 0.004 and 0.01, whereas the grasses, using the C_4 pathway, have *WUEs* that are about three times as high. Furthermore, there is an obvious relationship between *WUE* and $D_{s,b/g}$ for *Guiera* ($r^2 = 0.92$) and *Digitaria* ($r^2 = 0.94$), showing a sharp increase in *WUE* when $D_{s,b/g} < 20$ mbar, which does not hold for *Mitracarpus* ($r^2 = 0.04$).

4.6 Verification of the extended SVAT

The original SVAT model was run with measured values of L , measured soil heat flux, prescribed course of $r_{s,s}$ (dependent on day number) and root weighted soil moisture content, θ_r . Now, measured values of soil heat flux have been replaced by predictions with a soil model describing both soil heat and soil moisture transport. The predictions of soil moisture have been used to describe the dependency of $r_{s,s}$ on θ before the final rain storm ($r_{s,s} = 70\theta(1)^{0.87}$ instead of $r_{s,s} = 1000$, which caused poor predictions of $T_{s,i}$) and to update θ_r (see Eqn A11). The interactions and feedbacks between the atmosphere, vegetation and soil have been included by incorporating a simple growth model, driven by daily total net CO_2 uptake, and by allowing for soil water extraction by the roots of the upper and understorey. The ability of this new fully interactive model set-up to describe the actual course of L , θ and the energy and CO_2 fluxes and surface temperatures, will be briefly tested in the following paragraphs.

Soil

Fig. 12 compares the model predictions of soil moisture content in layers 1 and 2 with the data obtained from TDR and neutron probes. There appears to be a very good agreement between predictions and measurements during the entire period, supporting the reliability of soil hydraulic parameter estimates (see Table 3) and the root extraction function (Eqn 48).

Fig. 13 gives the measured and predicted courses of soil temperatures at these same levels. Again, agreement is good, indicating that the parameters describing soil heat transport (e.g. thermal conductivity) are fairly realistic. The correspondence between predicted and measured soil heat flux (see Fig. 16a) will provide the final verification of the soil model.

Vegetation

Fig. 14 shows the measured values (symbols) and model estimates (lines) of L for the three surface components. With the parameter estimates given in Table 1, needed in the growth module, the model is able to mimic the course of L during the 32 days. Note that L_b is virtually constant with time, while the largest increase in L is observed for the grasses.

Linked to the change in L is the change in leaf biomass. Fig. 15a compares the predicted and 'measured' (see Eqns 50 a and b which are based on a fit through the measurements) course in leaf biomass, W_{lv} , and stem (new wood), W_{sn} , biomass for the *Guiera senegalensis* shrubs. Increase in both leaf and new wood biomass is small and measurements and predictions correspond well. Fig. 15b gives the leaf and root biomass for the total herb undergrowth (herbs plus grasses). 'Measured' values of W_{lv} were calculated with Eqn 50c, whereas measured values of W_{rn} were taken from Fig. 2c by Hanan *et al.* (1997). Model estimates of leaf and root biomass are the sum of W_{lv} and W_{rn} as separately calculated for the herbs and grasses. Fig. 15 shows good agreement between model and reality.

Energy balance and CO_2 fluxes

Fig. 16 shows a comparison between predictions and measurements of the energy fluxes (Fig. 16a and b), the net CO_2 flux (Fig. 16c), and the bush and bare soil surface temperatures (Fig. 16d) for days 269 and 270 (25 and 26 September). Fig. 16a compares total net radiation, R_{nt} and soil heat flux, G_s . The latter was measured under a sparsely vegetated understorey plot (closed circles) and its predictions (solid line), obtained from the soil model, were used to estimate G for the bare soil ($1.0G_s$) and the herbs and grasses ($0.5G_s$). Agreement is good for both fluxes, both during daytime and nighttime. G_s is slightly underestimated. Reasonable agreement between model and measurements was also found for latent heat flux, λE , and sensible heat flux, H . The large scatter in the measured λE and H is caused by the sensitivity of the eddy correlation method to its necessary corrections (see Moncrieff *et al.* 1997). Predictions of F_c (Fig. 16c) are satisfactory, especially during the daytime.

Fig. 16d shows that the model is also able to estimate bush and soil surface temperature well, although a slight shift is now observed between the measured and predicted diurnal course of $T_{s,s}$, which is mainly caused by using calculated instead of measured soil heat flux. Table 6 shows the comparison between model predictions and measurements of energy balance fluxes R_n , G , λE and H , net CO_2 flux and bush and soil surface temperatures for all the half-hourly data available ($n = 913$). These values are comparable to those presented in Table 5, which supports the reliability of the predictions obtained with the extended SVAT.

Table 6. Statistics for comparison between model predictions and measurements of energy balance fluxes R_n , G , λE and H , net CO_2 flux and bush and soil surface temperatures ($n = 913$). The slope refers to the slope of a linear regression with zero intercept between data and predictions.

Variable	Slope	r^2
R_n	0.98	1.00
G	1.17	0.92
λE	0.82	0.90
H	0.75	0.81
F_c	0.67	0.77
$T_{s,b}$	1.02	0.87
$T_{s,s}$	0.98	0.93

4.7 Sensitivity analysis

Fig. 17 shows the effect of a doubling in atmospheric CO_2 concentration, C_a , a 1.5 °C increase in air temperature, T_a , and a combination of both on the total latent heat flux, λE (Fig. 17a), and on the predictions of λE_b (Fig. 17b), λE_h (Fig. 17c), λE_g (Fig. 17d) and λE_s (Fig. 17e). The solid line represents the reference run, the dotted line the doubling of C_a , the dashed line the results for the run with increased air temperature ($T_a + 1.5$), whereas the dashed-dotted line depicts the predictions when both driving variables are changed. The diurnal course shown in Fig. 17 is based on the average of the 32-day dataset ($n \approx 1490$ half-hourly flux estimates). A doubling of C_a leads to a considerable decrease in total λE , whereas a separate or combined increase in T_a has only a small effect (an increase in T_a causing a small increase in λE). The effect of a change in C_a , T_a or both variables on λE_b is comparable to that for total λE , but differences are much more pronounced. With a doubling in C_a , bush evaporation is only about one third of the original values. The considerable decrease in λE_b is predominantly caused by a similarly large decrease in bush stomatal conductance, as shown in Fig. 20a.

For the herbs, a totally different picture emerges, with a much smaller change in evaporation when the atmospheric driving variables are changed. In this case, an *increase* in C_a , T_a or both causes an *increase* in λE_h , with highest values observed when both C_a and T_a are changed. This is caused by the fact that, although stomatal conductance is significantly reduced by increased C_a and/or T_a (see Fig. 20b), the largely increased CO_2 uptake by the herbs (see Fig. 18c), causes a rapid increase in L_h (see Fig. 21b) which counteracts the potential decrease in evaporation caused by an increase in C_a .

The results for the grasses are comparable to those observed for the shrubs, again an increase in T_a clearly slightly favours evaporation, whereas a doubling of C_a , causing a severely reduced stomatal conductance (see Fig. 20c), lowers λE_g , this time by approximately 75%.

The bare soil evaporation is only slightly influenced by changes in atmospheric driving variables. In this case, increasing the air temperature has the largest influence.

Figure 18 shows the same comparison as given in Fig. 17, but this time for the CO_2 flux. Total net CO_2 uptake by the savannah system is obviously increased under

conditions of doubled atmospheric CO₂ concentration. An increase in T_r , however, causes a decrease in F_c as compared to the reference run, especially during midday. For the combined change in C_r and T_r , the early morning peak becomes more pronounced. The increase in F_c is mainly caused by the increased values of surface CO₂ concentration, C_s , which determines the driving force $C_s - C_i$ (see Eqn 7).

By contrast, the uptake of CO₂ by the bushes appears to be hardly affected by a doubling in C_r , with marginally higher values observed during early morning and late afternoon. An increase in T_r results in a lower uptake, while changing C_r and T_r simultaneously clearly reduces $P_{n,b}$, predominantly during the afternoon.

The effect of a changing environment on $P_{n,h}$ is entirely different; a scenario with a doubled CO₂ concentration, and an increase in both C_r and T_r , show a dramatic increase in $P_{n,h}$. The effect of T_r separately is very small and positive. Furthermore, no midday depression is observed.

For the grasses, the increase in net photosynthetic rate resulting from a doubling in C_r is relatively small, compared to the herbs. The effect of an increase in T_r is comparable, but negative.

The influence of the different scenarios on the efflux of CO₂ by the savannah, the soil respiration, is shown in Fig. 18e. The largest increase in R_{soil} is obtained with the combined scenario, giving an absolute increase of $\approx 0.1 \text{ mg m}^{-2} \text{ s}^{-1}$.

The changed values of latent heat flux and net photosynthetic rate will naturally influence the water use efficiency, WUE (see Eqn 51). It appeared that for all three species WUE roughly doubled when C_r was increased. The increase in WUE for the total savannah system was slightly less (80%), because of the counteracting effect of increased soil respiration for the $2C_r$ scenario. A rise in T_r lowered WUE slightly in all cases.

Fig. 19 shows the surface temperatures for the bushes, herbs, grasses and bare soil, respectively, under the four different climate scenarios. Largest differences are predicted for the bushes, especially when C_r and T_r are increased simultaneously ($\approx 5 \text{ }^\circ\text{C}$ increase in $T_{s,b}$). This is the result of the large drop in λE_b , as shown in Fig. 17b.

The maximum increase in surface temperature is much smaller for the herbs and the grasses, about 2-3 $^\circ\text{C}$ at the most. This is related to the smaller difference in λE between the four scenarios as compared to the bushes. The same applies to $T_{s,s}$.

Fig. 20 shows the average diurnal course of stomatal conductance for the three plant species. In all cases a similar pattern can be observed, with the highest conductances calculated for the reference case and the lowest for the combined case. Figs. 20 a and c show the largest reductions.

The effect of a different latent heat flux under the four scenarios is illustrated in Fig. 21, which plots the daily averaged soil moisture content of the first soil layer during days 251-283. Highest values are observed for the cases with increased C_r , when λE is lower (see Fig. 17a). For $T_r + 1.5$, θ is reduced, mainly as a result of increased λE .

Finally, Fig. 22 shows the effect of the changes in C_r and T_r on L_b , L_h and L_g , respectively. Changes in L_b are small, which is to be expected on the basis of Fig. 18b. Highest values are calculated for the $2C_r$ case, while lowest values are found for the $T_r + 1.5$ scenario. Fig. 22b shows a dramatic increase (50%) in L_h when C_r is doubled (with or without a simultaneous increase in T_r), which is linked to the results given in Fig. 18c. L_g , however, is only marginally influenced by the change in driving variables, and follows a similar course to the one depicted in Fig. 22a.

5. DISCUSSION

The least-square fitting procedure led to satisfactory estimates of the model parameters in the photosynthesis model of Jacobs *et al.* (1996). Although comparison material for the three savannah species is not available in the literature, the values of maximum photosynthetic rate, $P_{m,max}$, can roughly be verified using the information given by Wullschleger (1993), who lists values of the maximum rate of carboxylation, $V_{c,max}$, which approximately equals $2P_{m,max}$, for 109 C₃ species. According to Wullschleger, understorey herbs and forbs have a mean $V_{c,max}$ of 66 $\mu\text{mol m}^{-2} \text{s}^{-1}$ (range: 11-148 $\mu\text{mol m}^{-2} \text{s}^{-1}$). For *Mitracarpus*, $P_{m,max}$ equals 36 $\mu\text{mol m}^{-2} \text{s}^{-1}$ (equal to 1.6 $\text{mg m}^{-2} \text{s}^{-1}$, Table 1), which brings its $V_{c,max}$ (72 $\mu\text{mol m}^{-2} \text{s}^{-1}$) very close to 66. Wullschleger's average $V_{c,max}$ value for sclerophyllous shrubs is 53 $\mu\text{mol m}^{-2} \text{s}^{-1}$ (n=7, range: 35-71 $\mu\text{mol m}^{-2} \text{s}^{-1}$), so the *Guiera* $P_{m,max}$ (16 $\mu\text{mol m}^{-2} \text{s}^{-1}$) leads to a $V_{c,max}$ which is at the lower end of the range.

Figs. 2-4 show that the predictions of the total energy balance and CO₂ fluxes compare well with the measurements. The reliability of the micrometeorological fluxes used for verification of the model has been demonstrated in Gash *et al.* (1997), Lloyd *et al.* (1997) and Moncrieff *et al.* (1997). However, it is more difficult to check the separate component fluxes of λE_i , H_i and $P_{n,i}$ as predicted by the SVAT, because very few data of in-situ leaf photosynthesis and leaf evaporation were available. At the experimental site (CWS), two sapflow gauges were installed by the Winand Staring Centre, Wageningen, the Netherlands, around stems of *Guiera senegalensis* trees, to estimate bush transpiration. We compared the sapflow of the two gauges, measured between day 251 and 284, to the model predictions of λE_b . There was good agreement between the measured and predicted course of transpiration for both gauges ($r^2 = 0.91$ and 0.92, respectively), but the sapflow was on average only 75 and 66% of that predicted by the model for gauge 1 and gauge 2, respectively. The small number of gauges makes it difficult to decide if the model is overestimating. However, for a similar savannah, Allen & Grime (1995) found that the transpiration of the *Guiera* shrubs ($\alpha_b = 0.2$) was approximately 35% of the total evaporation for the whole season. This percentage compares well with our values presented in Figs. 3 and 7: if we plot model outcomes of $\alpha\lambda E_b$ against λE , we find that on average the bush transpiration equals 35% of the total evaporation ($r^2 = 0.99$), which supports our model estimates.

No measurements of leaf photosynthesis were available at this savannah site, but CO₂ fluxes at the leaf scale were recorded at the Southern Supersite (Levy *et al.* 1997), which was located at a distance of approximately 50 km from the CWS. The latter fallow bush site had not been planted with millet for about seven years and semi-natural vegetation similar to the one at the CWS, i.e. *Guiera senegalensis* shrubs with an understorey of grasses and herbs, had regrown. The leaf area index for the shrubs at the SSS increased from approximately 0.3 to 0.4 between days 250 and 280, which is comparable to the values observed at the CWS. Simultaneous measurements of leaf CO₂ flux and stomatal conductance were made using a portable open gas exchange system. Levy *et al.* (1997) find leaf CO₂ flux for *Guiera senegalensis*, as measured between July and October 1992 (the end of the HAPEX-Sahel campaign), to vary between 0 $\mu\text{mol m}^{-2} \text{leaf area s}^{-1}$ at 0 $\mu\text{mol m}^{-2} \text{s}^{-1}$ photosynthetic photon flux density (PPFD) and $\approx 8 \mu\text{mol m}^{-2} \text{leaf area s}^{-1}$ when PPFD reaches a maximum of 2000 $\mu\text{mol m}^{-2} \text{leaf area}$

s^{-1} . Highest values are observed when stomatal conductance is $> 150 \text{ mmol m}^{-2} s^{-1}$. These values are low compared to our SVAT predictions with maximum values for $P_{n,b}$ of around $0.8 \text{ mg m}^{-2} s^{-1}$ (the data shown in Fig. 10 were already multiplied by L_b and are on ground area basis not on leaf area basis). This equals $18 \text{ } \mu\text{mol m}^{-2} s^{-1}$, which is a factor 2-3 higher than the measurements obtained by Levy *et al.* (1997). Levy *et al.* (1997) find maximum leaf CO_2 fluxes of around $15 \text{ } \mu\text{mol m}^{-2} s^{-1}$ for the tigerbush tree species *Combretum nigricans* and *Combretum micranthum*, respectively, which is close to our value of $18 \text{ } \mu\text{mol m}^{-2} s^{-1}$. The differences between model predictions and measurements (at the SSS) may be because the two fallow sites were quite far apart with differences in soil conditions (moisture and nutrient status) and plant age (the shrubs at the SSS are thought to be a few years olders, which means leaf nitrogen content will be lower, and hence maximum photosynthetic rate will be less). Furthermore, stomatal conductance observed at the SSS was lower than the values measured at the CWS, which also might account for the difference. Also, Jacobs (1994) suggested that the considerable time (approximately 0.5-1.0 minute) during which a leaf is enclosed in a gas-exchange leaf chamber may cause reductions in observed leaf conductance and photosynthesis, because of the deprivation of light and changes in the local leaf environment.

Other comparison material can be found in the literature. Medina (1986) quotes maximum leaf photosynthesis rates of eight field grown or laboratory grown savannah trees ranging between $3.8 \text{ } \mu\text{mol m}^{-2} s^{-1}$ for *Ochna pulchra* and $11.8 \text{ } \mu\text{mol m}^{-2} s^{-1}$ for *Byrsonima crassifolia*. The average of the species (with no data for *Guiera senegalensis* present) is $8.4 \text{ } \mu\text{mol m}^{-2} s^{-1}$, but these data represent a mixture of species from several continents. Again, maximum leaf conductance of these species (Medina 1986), are low compared to the conductances obtained with porometry at the CWS for *Guiera senegalensis*. The observed overestimation of bush CO_2 exchange, and possibly of bush transpiration, may be because the model assumes that each component can be represented by a 'Big Leaf' approximation, receiving an average amount of radiation. To minimise computation time stratification of radiation, energy exchange etc. within the canopy was ignored. Hence radiative transfer within the canopy is not accounted for, which will especially influence the predictions for the *Guiera* bushes, as compared to the grasses and herbs, for which hardly any layering is observed.

Levy *et al.* (1997) also show leaf CO_2 flux data for the C_4 grass *Eragrostis tremula*. Although we used stomatal conductance data of *Digitaria guyana* to parameterise the photosynthesis of the grass component in the SVAT, the maximum CO_2 fluxes of the latter, being around $20 \text{ } \mu\text{mol m}^{-2} s^{-1}$, correspond well with the maximum leaf CO_2 flux shown in Levy *et al.* (1997) for *E. tremula*. Le Roux & Mordet (1995) obtained leaf CO_2 measurements on the dominant C_4 grass species *Hyparrhenia diplandra* in a West African humid savannah. They found that, despite their low nitrogen content, the leaves exhibited a remarkably high leaf photosynthetic capacity ($24 \text{ } \mu\text{mol m}^{-2} s^{-1}$ for $L = 1.5$). This corresponds well with maximum leaf photosynthesis reported for other humid or mesic savannah grass species which frequently exceeded $20 \text{ } \mu\text{mol m}^{-2} s^{-1}$, as shown in their Table 2. So far no data have been found in the literature of CO_2 fluxes of savannah herb or forb species, which hampers verification of the model predictions for $P_{n,h}$.

Confirmation of the modelled savannah soil respiration poses a similar problem: no soil CO_2 flux data were measured at the CWS and an attempt to quantify this flux at the SSS resulted in a very limited dataset, which has not been presented in the literature.

Fig. 10 shows that predicted peak soil CO₂ values at our site vary between 0.3 and 0.6 mg m⁻² s⁻¹, that is between 6.8 and 13.6 μmol m⁻² s⁻¹. For a humid savannah, Le Roux and Mordelet (1995) found soil respiration rates between 6.6 and 9.6 μmol m⁻² s⁻¹. These savannah values are relatively high compared to values quoted for soil respiration measured under different ecosystems in more temperate regions (e.g. Dugas *et al.* 1997). A high value of soil respiration at our savannah site may be warranted by the presence of termite activity, which has been reported to contribute largely to the soil carbon content and CO₂ flux (Darlington *et al.* 1997; De Bruyn & Conacher 1995).

WUE values given for the three species are within the range given in the literature for C₃ and C₄ species (Jones 1983). The higher values of *WUE_g*, as compared to *WUE_{b,h}*, are also supported by the literature: because of their lower C_i-values, C₄ plants are expected to have larger *WUE* than C₃ plants under similar environmental conditions (Jones 1983; Baldocchi 1994). The strong negative correlation between vapour pressure deficit and *WUE* has been reported before (Bierhuizen & Slatyer 1965; Schulze & Hall 1982; Baldocchi 1994; Baldocchi *et al.* 1985, Verhoef *et al.*, 1996a, although different mechanisms may be responsible for these similar results. For example, Baldocchi *et al.* (1985) see their relationship between atmospheric *D* and *WUE* ($r^2 = 0.71$) for a soybean crop as an artifact of water-stress-induced stomatal closure. They indeed found a strong decrease in *WUE* when stomatal resistance increased ($r^2 = 0.85$). In our case, *WUE_g* appeared to have only a weak dependence on $r_{s,i}$ (not shown): a negative correlation was found for *Guiera* ($r^2 = 0.53$), whereas for *Mitracarpus* and *Digitaria*, the dependence was slightly positive ($r^2 = 0.10$ and 0.16 , respectively). At the same time, both the bushes and the herbs exhibited strong water-stress-induced stomatal closure, when $r_{s,i}$ was plotted as a function of $D_{s,i}$ ($r^2 = 0.85$ and 0.80 , respectively, not shown). However, $r_{s,g}$ appeared to decrease weakly ($r^2 = 0.16$, not shown) with increasing $D_{s,g}$, but there was still a strong negative correlation between *WUE_g* and $D_{s,g}$ (see Fig. 11c). The lack of dependence of *WUE_h* on $D_{s,h}$ (see Fig. 11b), was also observed by Baldocchi (1994) when he plotted water use efficiency of a corn canopy against the absolute humidity of the atmosphere ($r^2 = 0.03$). In our case, this phenomenon can be explained by the fact that $g_{l,h}$ was largely influenced by soil moisture status, through multiplication with f_0 (see Appendix, description of Eqn A10-11). This caused the dependence of *WUE_h* on $D_{s,h}$ to shift upwards with decreasing soil moisture availability. If we split the datapoints depicted in Fig. 11b into three groups, with the most left cluster of data representing days 251-272 ($f_0 > 0.8$), the middle group *WUE* values between days 273-278 ($0.5 < f_0 < 0.8$), and the scattered right-hand data representing days 279-283 ($f_0 < 0.5$), a much clearer picture emerges with $r^2 = 0.83$, 0.77 and 0.42 for the three data clusters, respectively.

A variety of SVAT-type models has been described in the literature which in theory can produce simultaneous predictions of the energy balance and CO₂ exchange between a canopy and its environment. Several criteria can be used to distinguish between these models, with the most important ones being their spatial configuration, the approach used for the description of leaf conductance and CO₂ flux, and the type of output they concentrate on or the purpose they are used for.

Looking first at the spatial set-up of these models, in the simplest the vegetation is described by a Big-Leaf model (Jacobs *et al.* 1996; Cox *et al.* 1997). In the others, the models allow for vertical or horizontal heterogeneity. The first group, consisting of models featuring many canopy layers which mainly differ in the amount of radiation they

receive, allow the behaviour of a relatively closed, tall canopy, such as a forest in the temperate regions to be described. Examples of SVATs describing such one-dimensional, multi-layer systems can, for example, be found in Sellers *et al.* (1992), Baldocchi & Harley (1995). When a canopy is more spatially inhomogeneous, a multi-source description has proven indispensable. A number of two-source models can be found in the literature (e.g. Lynn & Carlson 1990; Carlson & Bunce 1996; Chen *et al.* 1996; Oliosio *et al.* 1996) describing the energy balance and CO₂ flux of a two-source surface consisting of a main canopy and an understorey of herbs or bare soil.

Another feature that distinguishes the SVATs from each other is the way in which they parameterise leaf conductance or CO₂ flux or both. In some models both leaf conductance and CO₂ flux are parameterised using empirical, multiplicative factors depending on environmental conditions such as light, atmospheric humidity, temperature etc. (e.g. Oliosio *et al.* 1996). In the others they are determined by physiological descriptions (Jacobs *et al.* 1996; Harley & Baldocchi 1995; Chen *et al.* 1996) and photosynthesis and stomatal opening are directly related. Sometimes a mixture of the empirical and physiological approach is employed (Lynn & Carlson 1990; Oliosio *et al.* 1996).

Furthermore, the various SVATs have been developed for a variety of purposes. Some of them are used for the description of the diurnal variation in fluxes and mainly use a combination of micro-meteorological and plantphysiological data (Baldocchi & Harley 1995; Oliosio *et al.* 1996). For example, Oliosio *et al.* (1996) compared two SVATs in their ability to simulate the diurnal course of photosynthesis and transpiration, especially the photosynthetic midday depression and the transpiration plateau, for a soybean crop undergoing water stress. Others have to be regarded as ecosystem models, linking biochemical, ecophysiological and ecosystem processes and focusing on long-term predictions. For example, Chen *et al.* (1996), used their GEM2 model to describe successfully the long-term variation in biomass (shoot & root) of two grass species (*Pascopyrum smithii* and *Bouteloua gracilis*) under different treatments (increased atmospheric CO₂ concentration, increased temperature and increased precipitation). In their paper, no verification of the energy balance or surface temperatures took place. In other studies, SVATs, sometimes coupled to a planetary boundary layer model, are employed to perform sensitivity analyses to study the effect of climate change and CO₂ enrichment on terrestrial vegetation (e.g. Carlson & Bunce 1996).

Our SVAT falls in the multi-source category, but it has the added advantage of allowing for more than just two sources and it simultaneously describes and links the energy balance, net CO₂ exchange and surface temperature, using a physiological description of leaf conductance. In many studies a concurrent check of surface temperature is often ignored (Baldocchi & Harley, 1995; Oliosio *et al.* 1996). Furthermore, CO₂ exchange occurs through the same resistance network as sensible heat and water vapour, as opposed to Chen *et al.* (1996), for example. Respiration and CO₂ exchange with the soil are often not taken into account (Oliosio *et al.* 1996), which may cause unreliable predictions if the model in question were used for a sensitivity analysis, for example.

Runs with the extended model, i.e. the SVAT with a description of growth and soil heat/water transfer incorporated, showed that simulated and observed soil moisture content, soil temperature, soil heat flux, leaf area index, biomass and atmospheric fluxes/surface temperature compared favourably.

The sensitivity analysis performed with this extended SVAT revealed that elevated CO₂ concentration enhanced average net CO₂ uptake of the savannah system by 60%,

decreased total evaporation by 15%, increased leaf biomass by 30% for the total herb layer, and increased leaf stomatal resistance by values ranging between 50% (herbs) and 150% (bushes). Many studies indeed show that a doubling of CO₂ results in an increase in carbon exchange rate between the plant and the atmosphere, an increase in stomatal resistance, and a decrease in transpiration. Cure and Acock (1986), for example, published a literature survey of measurements pertaining to the effects of CO₂ doubling on transpiration (-20%), biomass (+30%), carbon assimilation rate (+ 50%) and stomatal resistance (+25%) for 10 non-forage crops, using single leaves or isolated plants. Most of their values correspond well to our estimates for the savannah, although our increase in stomatal resistance was considerably higher. Jarvis's (1989) estimates are also in accord with these values.

The effect of elevated CO₂ on transpiration and CO₂ uptake can not be generalised. The effect on transpiration is often believed to be overestimated for single plant experiments, as compared to plants in field conditions. Furthermore, for some species, higher transpiration rates are observed, despite increase in stomatal resistance (Nijs *et al.* 1988). The same phenomenon was observed for the *Mitracarpus* herbs.

CO₂ enrichments studies also show different responses of CO₂ uptake in different systems. Chen *et al.* (1996) report that in tussock tundra, the stimulation of carbon assimilation differed largely during three consecutive years. In estuary marsh, elevated CO₂ strongly stimulated C₃ species photosynthesis and growth, but C₄ species responded only slightly. In a tallgrass prairie, however, the production of a C₄ grass showed a greater response to elevated CO₂ than that of C₃ plants. Different responses might be due to differences in temperature, soil water and nutrient availability. Simulation modelling indicated that the interactions among environmental variables, as well as the main effects of CO₂ enrichment, were important in determining whole ecosystem responses to CO₂ enrichment and climate change (Chen *et al.* 1996).

It appeared that for all three species *WUE* roughly doubled when C_i was increased. A rise in T_r lowered *WUE* slightly in all cases. These findings are consistent with Drake *et al.* (1997).

6. CONCLUSIONS

The results presented in this paper show that a calibrated SVAT, consisting of a physiologically-based leaf conductance model, which has been embedded in a four-component Penman-Monteith energy partitioning description, can satisfactorily ($0.81 \leq r^2 \leq 0.99$) predict the diurnal variation of the energy balance, surface temperatures and net CO₂ exchange of a Sahelian savannah for a 30-day period during which atmospheric, vegetation and soil conditions significantly varied. Flux and surface temperature predictions of the four surface components illustrate various interesting interactions between the plant species and the soil. Calculated water use efficiencies for the vegetation have plausible values for C₃ and C₄ species and show a strong dependency on vapour pressure deficit, which confirms findings by e.g. Baldocchi (1994).

Various canopy models have been presented in literature that successfully describe the energy fluxes and net CO₂ uptake of a certain ecosystem. However, in several cases (e.g. Baldocchi & Harley 1995), horizontal homogeneity is assumed which means that the model is a useful tool for the description of a one-dimensional, multi-layer canopy such as a temperate forest, but not for a horizontally heterogeneous sparse canopy. For SVAT models that allow for spatial inhomogeneity, often (e.g. Carlson & Bunce 1996; Olioso *et al.* 1996) no inter-regulations between photosynthesis and leaf conductance are taken into account and leaf conductance is still parameterised using empirical multiplicative factors. Additionally, as far as we can see the maximum number of sources or components in those models is two, which hampers reliable simulation of those surfaces consisting of multi-species upper or understories. Where several species are present, distinguishing between just two components is simply not enough and may lead to unrealistic parameterisations and predictions. Although, partly through calibration, satisfactory agreement can be found between data and model estimates, models like these will probably produce less reliable results if they are used for climate change studies, for example (see Carlson & Bunce 1996).

This new model appears to be able to simulate the complex interactions between CO₂, water and heat fluxes in multi-component vegetation. With a simple growth model linked to it, translating the uptake of CO₂ in a change in leaf area index, it has been used to investigate the effect of climate change and CO₂ enrichment in a mixed-species savannah ecosystem. This sensitivity analysis indicated that elevated CO₂ concentration enhanced average net CO₂ uptake of the savannah system by 60%, decreased total evaporation by 15%, increased leaf biomass by 30% for the total herb layer, and increased leaf stomatal resistance by values ranging between 50% (herbs) and 150% (bushes). *WUE* roughly doubled. The effect of a 1.5 °C increase in air temperature was usually small compared to the CO₂ doubling.

However, the contribution of the different ecosystem components to the net decrease in ecosystem evaporation and the increase in CO₂ uptake was very different. While for the bushes (C₃) and the grasses (C₄) a large decrease in evaporation was observed, the herbs (C₃) showed a small increase in evaporation with CO₂ doubling. On the other hand, the uptake of CO₂ by the bushes and the grasses was only little affected, whereas that for the herbs was more than doubled. This large increase in CO₂ uptake for the herbs caused leaf area index (via the growth model) to rise sharply, hence counteracting the negative effect of increased stomatal resistance, which occurred for all three species under conditions of elevated CO₂. Despite their variable behaviour, *WUE* doubled for all three

species, when CO₂ concentration was increased. The surface temperatures of the three species were mainly affected in relation to their change in evaporation (lower evaporation resulting in higher surface temperatures), with the largest increase for the scenario where CO₂ concentration and air temperature were increased simultaneously. This interaction is important because surface temperature plays an important role in the processes of photosynthesis and stomatal opening.

These results illustrate the intricate interplay between changing CO₂ uptake, leaf area index, evaporation and surface temperature, which can only be simulated with a mechanistic model where physiological and meteorological processes are closely linked thus allowing for the interaction and feedbacks between the different processes and ecosystem components. We conclude that more experimental and modelling efforts are needed to address the possible effects of CO₂ enrichment and climate change on the competitive balance between different species in a plant community. A multi-component, mechanistic model, like the one described in this report, will be a valuable tool for this purpose. Such a model can also be employed in research concerning productivity and water use efficiency in mixed crops, such as agroforestry systems.

ACKNOWLEDGEMENTS

I want to thank Simon Allen, Robin Hall, John Roberts and Chris Huntingford for their valuable contributions to this report. Furthermore, I am grateful to my ex-colleagues and students at the Department of Meteorology, Wageningen, the Netherlands for enabling me to establish the extended and high-quality dataset used in this report.

APPENDIX 1

This appendix describes how the net photosynthetic rate, $P_{n,i}$, and the leaf stomatal resistance, $r_{s,i}$, are calculated for the plant components in the SVAT. Throughout the appendix, subscripts i , used to denote component $i = b$ (bushes), h (herbs), or g (grasses) have been omitted for reasons of simplicity.

To solve the relationship between the net photosynthetic rate of plants and their leaf stomatal resistance, as given in Eqn 3, we need an expression for the internal CO₂ concentration, C_i . Experimental evidence (see Jacobs *et al.* 1996) has shown that the ratio between C_i and C_a is fairly constant:

$$\frac{C_i}{C_a} = k \quad (\text{A.1})$$

The parameter k (-) is given by

$$k = f + (1 - f) \frac{\Gamma}{C_a} \quad (\text{A.2})$$

where Γ (mg m⁻³) is the CO₂ compensation concentration which is parameterised as a function of temperature:

$$\Gamma = \Gamma(@25) * 1.5^{0.1(\tau_s - 25)} \quad (\text{A.3})$$

where $\Gamma(@25)$ is the CO₂ compensation concentration at 25 °C, which has been set to 80 and 5 mg m⁻³ for C₃ and C₄ plants, respectively. Γ is low for C₄ plants, because in these plants the light respiration process does not occur (see Jacobs *et al.* 1996).

f (-) is a function of the specific humidity deficit at leaf level, D_s (mbar):

$$f = f_0 \left(1 - \frac{D_s}{D_{s,\max}} \right) \quad (\text{A.4})$$

where f_0 (-) is the value of f at $D_s = 0$ and $D_{s,\max}$ (mbar) is the value of D_s , where the stomata are completely closed.

An empirical light response curve is used to combine the influence of CO₂ and light on P_n (mg m⁻² s⁻¹):

$$P_n = (P_m + R_{\text{dk}}) \left(1 - \exp\left(\frac{-\epsilon I_a}{P_m + R_{\text{dk}}} \right) \right) - R_{\text{dk}} \quad (\text{A.5})$$

where the dark respiration, R_{dk} (mg m⁻² s⁻¹), is $P_m/9$. P_m (mg m⁻² s⁻¹) is the photosynthetic rate at saturating light intensity and I_a (W m⁻²) is the absorbed PAR, which is given by

$$I_a = (1 - 0.15) * 0.5 R_{\text{sol}} / L^* \quad (\text{A.6})$$

where 0.15 is the leaf reflectivity, R_{sol} the incoming solar radiation ($W m^{-2}$), L^* the local leaf area index and the factor 0.5 is necessary for conversion to PAR expressed in $W m^{-2}$.

The initial quantum use efficiency, ε ($mg J^{-1} PAR$), quantifying the slope of the light response curve can be expressed as

$$\varepsilon = \varepsilon_0 \frac{C_s - \Gamma}{C_s + 2\Gamma} \quad (A.7)$$

The maximum quantum use efficiency, ε_0 , will be taken as 0.017 for C_3 plants and 0.014 $mg J^{-1} PAR$ for C_4 species (see Jacobs 1994). P_m is found from

$$P_m = P_{m,max} \left(1 - \exp \left(\frac{-g_m (C_i - C_s)}{P_{m,max}} \right) \right) \quad (A.8)$$

whereas $P_{m,max}$ and the mesophyll conductance, g_m ($m s^{-1}$), are given by

$$X(T_s) = \frac{X(@25) * 2^{0.1(T_s-25)}}{(1 - \exp 0.3(T_1 - T_s))(1 - \exp 0.3(T_2 - T_s))} \quad (A.9)$$

where $X(T)$ is either $P_{m,max}$ or g_m , at any leaf surface temperature T_s , with specific values of $X(@25)$, and reference temperature T_1 and T_2 . $X(@25)$ is the value of X at 25 °C.

The dependency of leaf stomatal conductance on soil moisture was parameterised using a linear multiplication factor, f_θ , which ranges between 0 (very low soil moisture status) and 1.0 (ample soil moisture available):

$$f_\theta = 1 - \frac{(\Psi_{max} - \Psi_r)}{\Psi_{max} - c} \quad (A10)$$

in which Ψ_r and Ψ_{max} are the average root-weighted soil water potential and the soil water potential at field capacity respectively. The latter is taken at -0.39 m. Ψ_r is a function of root-weighted volumetric soil moisture content, θ_r , which was parameterised as

$$\ln(-\Psi_r) = -0.4059 - 2.0556 \ln \theta_r \quad (A11)$$

θ_r was found by integrating soil moisture profiles weighted by root distributions of *Guiera* and the undergrowth measured in the field (see Eqn 47). For the calibration run measured soil moisture was taken, while for the extended SVAT estimates of θ in the 5 soil layers were used. The estimate of g_i , as obtained from the equations above, was multiplied by f_θ to incorporate the dependence on soil moisture in the final model predictions of r_i .

REFERENCES

- Allen, S.J., & Grime, V.L. (1995) Measurements of transpiration from savannah shrubs using sapflow gauges. *Agricultural and Forest Meteorology* **75**, 23-41.
- Baldocchi, D. (1994) A comparative study of mass and energy exchange over a closed C₃ (wheat) and an open C₄ (corn) crop: II CO₂ exchange and water use efficiency. *Agricultural and Forest Meteorology* **67**, 291-321.
- Baldocchi, D., Verma, S.B. & Rosenberg, N.J. (1985) Water use efficiency in a soybean field: influence of plant water stress. *Agricultural and Forest Meteorology* **34**, 53-65.
- Baldocchi, D.D. & Harley, P.C. (1995) Scaling carbon dioxide and water vapour exchange from leaf to canopy in a deciduous forest. II. Model testing and application. *Plant, Cell and Environment* **18**, 1157-1173.
- Ball, J.T., Woodrow, I.E. & Berry, J.A. (1987) A model predicting stomatal conductance and its contribution to the control of photosynthesis under different environmental conditions. In: J. Biggins (Ed.), *Progress in Photosynthesis Research*, Vol. IV. Martinus Nijhoff Publishers, Dordrecht, 221-224.
- Bierhuizen, J.F. & Slatyer, R.O. (1965) Effects of atmospheric concentration of water vapour and CO₂ in determining transpiration photosynthesis relationships of cotton leaves. *Agricultural and Forest Meteorology* **2**, 259-270
- Breman, H., & Kessler, J-J (1995) Woody plants in agro-ecosystems of semi-arid regions. *Advanced Series in Agricultural Sciences* **23**. Springer Verlag, Berlin, 340 pp.
- Brutsaert, W. (1975) On a derivable formula for long-wave radiation from clear skies. *Water Resources Research* **11**, 742-744.
- Carlson, T.N. & Bunce, J.A. (1996) Will a doubling of atmospheric carbon dioxide concentration lead to an increase or a decrease in water consumption by crops ? *Ecological Modelling* **88**, 241-246.
- Chen, D., Hunt, H.W. & Morgan, J.A. (1996) Responses of a C₃ and C₄ perennial grass to CO₂ enrichment and climate change: Comparison between model predictions and experimental data. *Ecological Modelling* **87**, 11-27.
- Choudhury, B.J. & Monteith, J.L. (1988) A four-layer model for the heat budget of homogeneous land surfaces. *Quarterly Journal of the Royal Meteorological Society* **114**, 373-398.
- Cox, P.M., Huntingford, C. & Harding, R.J. (1997) A canopy conductance and photosynthesis model for use in a GCM land surface scheme. *Journal of Hydrology in press*.

Cuenca, R.H., Brouwer, J., Chanzy, A., Droogers, P., Galle, S., Gaze, S.R., Sicot, M., Stricker, H., Angulo-Jaramillo, R., Boyle, S.A., Bromley, J., Chebhouni, A.G., Cooper, J.D., Dixon, A.J., Fies, J.-C., Gandah, M., Gaudu, J.-C., Laguerre, L., Lecocq, J., Soet, M., Steward, H.J., Vandervaere, J.-P. & Vauclin, M. (1997) Soil measurements during HAPEX-Sahel intensive observation period. *Journal of Hydrology* 188-189, 224-266.

Cure, J.D. & Acock, B. (1986) Crop responses to carbon dioxide doubling: a literature survey. *Agricultural and Forest Meteorology* 38, 127-145.

Darlington, J.P.E.C., Zimmerman, P.R., Greenberg, H.J., Westberg, C. & Bakwin, P. (1997) Production of metabolic gases by nests of the termite *Marcotermes jenneli* in Kenya. *Journal of Tropical Ecology* 13, 491-510.

Deardorff, J.W. (1978) Efficient prediction of ground surface temperature and moisture, with inclusion of a layer of vegetation. *Journal of Geophysical Research* 83, 1889-1903.

De Bruyn, L.A.L. & Conacher, A.J. (1995) Soil modification by termites in the central wheat-belt of Western-Australia. *Australian Journal of Soil Research* 33, 179-193.

Dolman, A.J. (1993) A multiple-source land surface energy balance model for use in general circulation models. *Agricultural and Forest Meteorology* 65, 21-45.

Drake, B.G., Gonzalez Meler, M.A. & Long, S.P. (1997) More efficient plants: A consequence of rising atmospheric CO₂? *Annual Review of Plant Physiology and Plant Molecular Biology* 48, 609-639.

Dugas, W.A., Reicosky, D.C. & Kiniry, J.R. (1997) Chamber and micrometeorological measurements of CO₂ and H₂O fluxes for three C₄ grasses. *Agricultural and Forest Meteorology* 83, 113-133.

Gash, J.H.C., Kabat, P., Monteny, B.A., Amadou, M., Bessemoulin, P., Billing, H., Blyth, E.M., de Bruin, H.A.R., Elbers, J.A., Friborg, T., Harrison, G., Holwill, C.J., Lhomme, J.-P., Moncrieff, J.B., Puech, D., Soegaard, H., Taupin, J.D., Tuzet, A. & Verhoef, A. (1997) The variability of evaporation during the HAPEX-Sahel Intensive Observation Period. *Journal of Hydrology* 188-189, 385-399.

Goudriaan, J., Van Keulen & Van Laar, H.H. (1992) Crop growth model for potential production (SUCROS1). In: Van Laar, H.H., Goudriaan, J. & Van Keulen, H. (Eds.) *Simulation of crop growth for potential and water-limited production situations (as applied to spring wheat)*, Department of Theoretical Production Ecology (TPE-WAU), DLO Centre for Agrobiological Research (CABO-DLO), p. 1-25.

Goutorbe, J.-P., Lebel, T., Tinga, A., Bessemoulin, P., Brouwer, J., Dolman, A.J., Engman, E.T., Gash, J.H.C., Hoepffner, M., Kabat, P., Kerr, Y.H., Monteny, B., Prince, S., Said, F., Sellers, P. & Wallace, J.S. (1994) HAPEX-Sahel: a large scale study of land atmosphere interactions in the semi-arid tropics. *Annales Geophysicae* 12, 53-64

Hanan, N.P., & Prince, S.D. (1997) Stomatal conductance of West Central Supersite vegetation in HAPEX-Sahel: measurements and empirical models. HAPEX-Sahel special issue, *Journal of Hydrology* **188-189**, 536-562.

Hanan, N.P., Prince, S.D. Bégué, A. (1997) Modelling vegetation primary production during HAPEX-Sahel using production efficiency and canopy conductance model formulations. *Journal of Hydrology* **188-189**, 651-675.

Harley, P.C. & Baldocchi, D.D. (1995) Scaling carbon dioxide and water vapour exchange from leaf to canopy in a deciduous forest. I. Leaf model parameterization. *Plant, Cell and Environment* **18**, 1146-1156.

Huntingford, C., Allen, S.J. & Harding, R.L. (1995) An intercomparison of single and dual-source vegetation-atmosphere transfer models applied to transpiration from Sahelian savannah. *Boundary-Layer Meteorology* **74**, 397-418.

Jacobs, C.M.J. (1994) Direct impact of atmospheric CO₂ enrichment on regional transpiration. Department of Meteorology, WAU, the Netherlands, 179 p.

Jacobs, C.M.J., van den Hurk, B.J.J.M. & de Bruin, H.A.R. (1996) Stomatal behaviour and photosynthetic rate of stressed grapevines in semi-arid conditions. *Agricultural and Forest Meteorology* **80**, 111-134.

Jarvis, P.G. (1989) Atmospheric carbon dioxide and forests. *Phil. Trans. R. Soc. Lond., B*. **324**, 369-392.

Jones, H.G. (1983) Plants and microclimate. Cambridge: Cambridge University Press, pp. 323.

Kabat, P., Prince, S.D. & Prihodko, L., (Editors) (1996). HAPEX-Sahel West Central Supersite: Methods, Measurements and Selected Results. *Report 130*, DLO Winand Staring Centre, Wageningen.

Lebel, T., Taupin, J.D. & Amato, N.D. (1997) Rainfall monitoring during HAPEX-Sahel. 1. General rainfall conditions and climatology. *Journal of Hydrology* **188-189**, 74-96.

Le Roux, X. & Mordelet, P. (1995) Leaf and canopy CO₂ assimilation in a West African humid savanna during the early growing season. *Journal of Tropical Ecology* **11**, 529-545.

Leuning, R. (1995) A critical appraisal of a combined stomatal-photosynthesis model for C₃ plants. *Plant, Cell and Environment* **18**, 339-355.

Levy, P.E., Moncrieff, J.B., Massheder, Jarvis, P.G., J.M., Scott, S.L. & Brouwer, J. (1997) CO₂ fluxes at leaf and canopy scale at the HAPEX-Sahel southern super-site. *Journal of Hydrology* **188-189**, 612-632.

- Lloyd, C.R., Bessemoulin, P., Copley, F., Culf, A.D., Dolman, A.J., Elbers, J., Heusinkveld, B., Moncrieff, J., Monteny, B. & Verhoef, A. (1997) An intercomparison of surface flux measurements during HAPEX-Sahel. *Journal of Hydrology* **188-189**, 400-425.
- Lynn, B. & Carlson, T.N. (1990) A model illustrating plant versus external control of transpiration. *Agricultural and Forest Meteorology* **52**, 5-43.
- Medina E. (1986) Forests, savannas and montane tropical environments. In: Baker N.R., Long S.P. (Editors). *Photosynthesis in contrasting environments*. Elsevier, Amsterdam, 139-171.
- Moncrieff, J.B., Monteny, B., Verhoef, A., Friborg, Th., Elbers, J.H., Kabat, P., de Bruin, H.A.R., Soegaard, H., Jarvis, P.G. & Taupin, J.D. (1997) Spatial and temporal variations in net carbon flux during HAPEX-Sahel. *Journal of Hydrology* **188-189**, 563-588.
- Monteith, J.L. (1965) Evaporation and environment. In G. E. Fogg, (ed.) *The State and Movement of Water in Living Organisms*, Sympos. Soc. Exper. Biol., Vol. **19**, Academic Press, N.Y., pp. 205-234.
- Nijs, I., Impens, I. & Behaeghe, T. (1988) Effects of rising atmospheric carbon dioxide concentration on gas exchange and growth of perennial ryegrass. *Photosynthetica* **22**, 44-50.
- Norman, J.M., Garcia, R. & Verma, S.B. (1992) Soil surface CO₂ fluxes and the carbon budget of a grassland. *Journal of Geophysical Research* **97**, 845-853.
- Olioso, A., Carlson, T.N. & Brisson, N. (1996) Simulations of diurnal transpiration and photosynthesis of a water stressed soybean crop. *Agricultural and Forest Meteorology* **81**, 41-59.
- Raats, P.A.C. (1970) Steady infiltration from line sources and furrows. *Soil Science Society of America Proceedings* **34**, 709-714.
- Rozema, J., Lambers, H., van de Geijn, S.C., & Cambridge, M.L. (1993) *CO₂ and the Biosphere*, Kluwer Academic Publishers, Dordrecht, The Netherlands.
- Schulze, E.-D., & Hall, A.E. (1982) Stomatal responses, water loss and CO₂ assimilation rates of plants in contrasting environments. In: O.L. Lange, P.S. Nobel, C.B. Osmond and H. Ziegler (Editors), *Encyclopedia of Plant Physiology*, New Series, Vol. **12B**, Physiological Plant Ecology II. Springer Verlag, Berlin, pp. 181-230.
- Sellers, P.J., Mintz, Y., Sud, Y.C., & Dalcher, A. (1986) A simple biosphere model for use within general circulation models. *Journal of Atmospheric Science* **43**, 505-531.
- Sellers, P.J., Berry, J.A., Collatz, G.J., Field, C.B. & Hall, F.G. (1992) Canopy reflectance, photosynthesis, and transpiration. III. A reanalysis using improved leaf

models and a new canopy integration scheme. *Remote Sensing of Environment* 42,187-216.

Shuttleworth, W. J. & Wallace, J.S. (1985) Evaporation from sparse crops-an energy combination theory. *Quarterly Journal of the Royal Meteorological Society* 111, 839-855.

Soet, M., Droogers, P., Jaarsma, M.N., Kim, C.P, Monincx, J.F. & Stricker, J.N.M. (1995) HAPEX-Sahel: Basic description of methods and datasets. *Rapport 43, Vakgroep Waterhuishouding, Wageningen, the Netherlands*, 50 p.

Spitters, C.J.T., Van Keulen, H. & Van Kraalingen, D.W.G. (1989) A simple and universal crop growth simulator: SUCROS87. In: R. Rabbinge, S.A. Ward & H.H. van Laar (Eds.). Simulation and systems management in crop protection. *Simulation Monograph* 32, Pudoc, Wageningen, the Netherlands, pp. 147-181.

Stroosnijder, L. (1982) Le milieu Sahélien et les terrains expérimentaux. In: *La productivité des pâturages Sahéliens*, F.W.T. Penning de Vries et M.A. Djitéye (Editors), Pudoc, Wageningen.

Ten Berge, H.F.M (1990) Heat and water transfer in bare topsoil and the lower atmosphere. *Simulation Monographs* 33. Pudoc Wageningen, the Netherlands, 207 p.

Van Keulen, H., Penning de Vries, F.W.T., & Drees, E.M. (1982) A summary model for crop growth. In: F.W.T. Penning de Vries & H.H. van Laar. Simulation of plant growth and crop production. *Simulation monographs*, Pudoc, Wageningen, the Netherlands, pp. 87-97.

Verhoef, A. (1995) Surface energy balance of shrub vegetation in the Sahel. PhD-thesis, Dept. of Meteorology, Wageningen Agricultural University, Wageningen, the Netherlands, ISBN 90-5485-458-8, 247 pp.

Verhoef, A. (1997) The effect of temperature differences between porometer head and leaf surface on stomatal conductance measurements. *Plant, Cell & Environment* 20, 641-646.

Verhoef, A., Allen, S.J., De Bruin, H.A.R., Jacobs, C.M.J. & Heusinkveld, B. (1996a) Fluxes of carbon dioxide and water vapour from a Sahelian savanna. *Agricultural and Forest Meteorology* 80, 231-248.

Verhoef, A., Van den Hurk, B.J.J.M, Jacobs, A.F.G. & Heusinkveld, B. G. (1996b) Thermal soil properties for a vineyard (EFEDA-I) and a savanna (HAPEX-Sahel) site. *Agricultural and Forest Meteorology* 78, 1-18.

Verhoef, A., McNaughton, K.G., & Jacobs, A.F.G. (1997) A parameterization of momentum roughness length and displacement height for a wide range of canopy densities. *Hydrology and Earth Systems Sciences* 1, 81-91.

Wullschleger, S.D. (1993) Biochemical limitations to carbon assimilation in C3 plants- a retrospective analysis of the A/C_i curves from 109 species. *Journal of Experimental Botany* 44, 907-920.

4) UNEXPECTED DEVELOPMENTS, RESULTS OR CONCLUSIONS NOT FORESEEN AT THE ONSET OF THE TRAINING PERIOD

(maximum 10 lines):

For the sparse savannah, soil respiration and photosynthesis are of similar magnitude. An initial problem is that direct measurements of soil respiration are not available. First attempts to model soil respiration as a function of soil temperature and soil moisture show that only a relatively small percentage of the variance in nighttime CO₂ fluxes can be explained.

5) RESEARCH LINES AND/OR RESEARCH APPROACHES WHICH PROVED TO BE UNSUCCESSFUL (maximum 2 pages):

Not applicable

6) PUBLICATIONS

Verhoef, A. (1997) The effect of temperature differences between porometer head and leaf surface on stomatal conductance measurements. *Plant, Cell & Environment* **20**, 641-646.

Verhoef, A. & Allen, S.J. (1998) The relative importance of surface and aerodynamic resistances in a multisource energy-CO₂ model applied to Sahelian savannah. *Physics and Chemistry of the Earth*, in press.

Verhoef, A. & Allen, S.J. (1998) SVAT model describing energy and CO₂ fluxes for multi-component vegetation: calibration and test for a Sahelian savannah. *Plant, Cell & Environment*, submitted.

Verhoef, A. & Hall, R.L. (1998) A multi-component model of energy and CO₂ exchange of a Sahelian savannah: sensitivity to CO₂ enrichment and climate change. *Ecological Modelling*. In preparation.

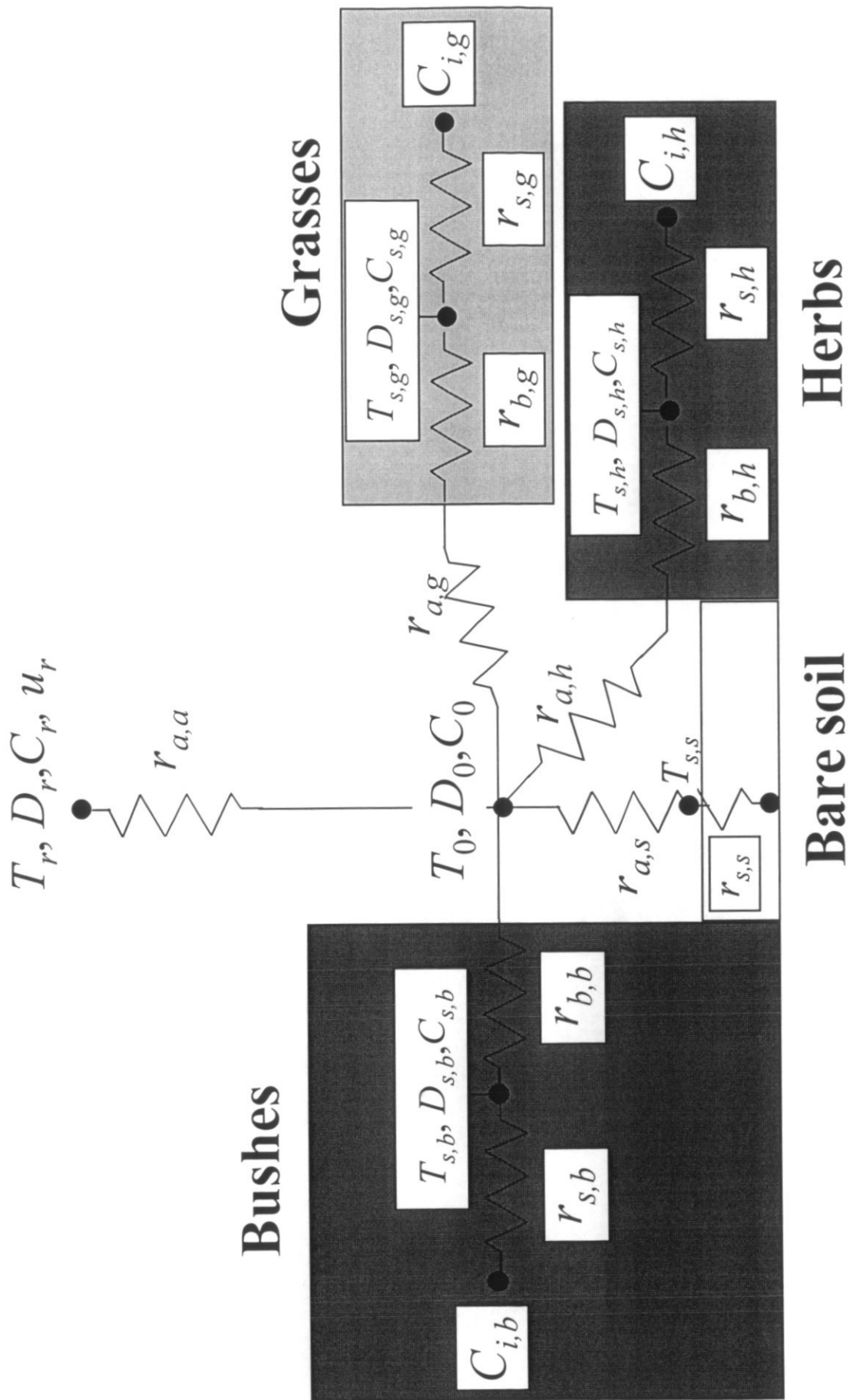


Figure 1. Schematic representation of the multi-component energy-CO₂ model.

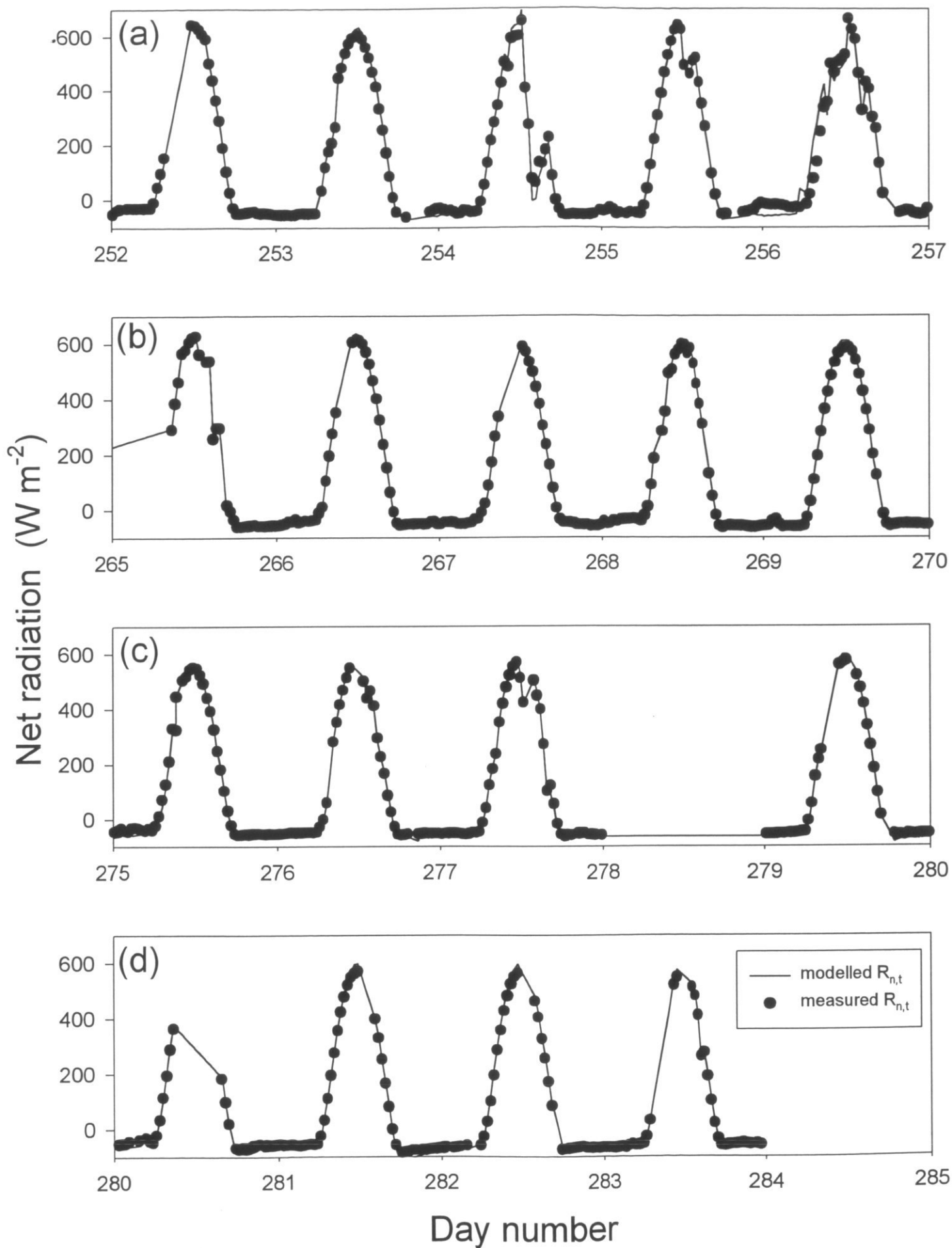


Figure 2. A comparison between measured (closed circles) and modelled (solid lines) total net radiation for a) days 252-256 (wet period), b) days 265-269 (just after the last rainfall), c) days 275-279 (dry-down), d) days 280-284 (start of senescence).

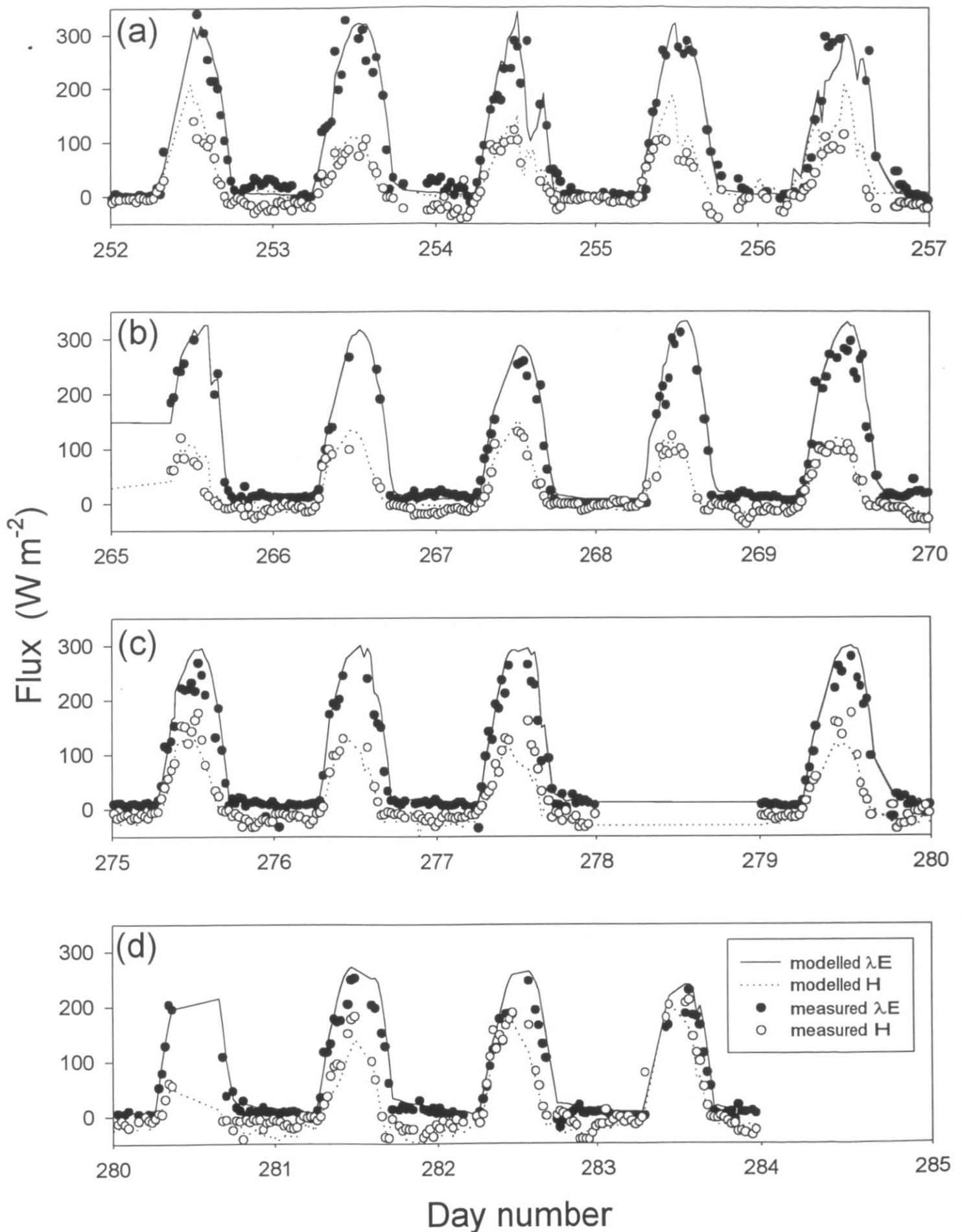


Figure 3. A comparison between measured (closed circles) and modelled (solid lines) total evapotranspiration and measured (open circles) and modelled (dotted lines) total sensible heat flux total for a) days 252-256 (wet period), b) days 265-269 (just after the last rainfall), c) days 275-279 (dry-down), d) days 280-284 (start of senescence).

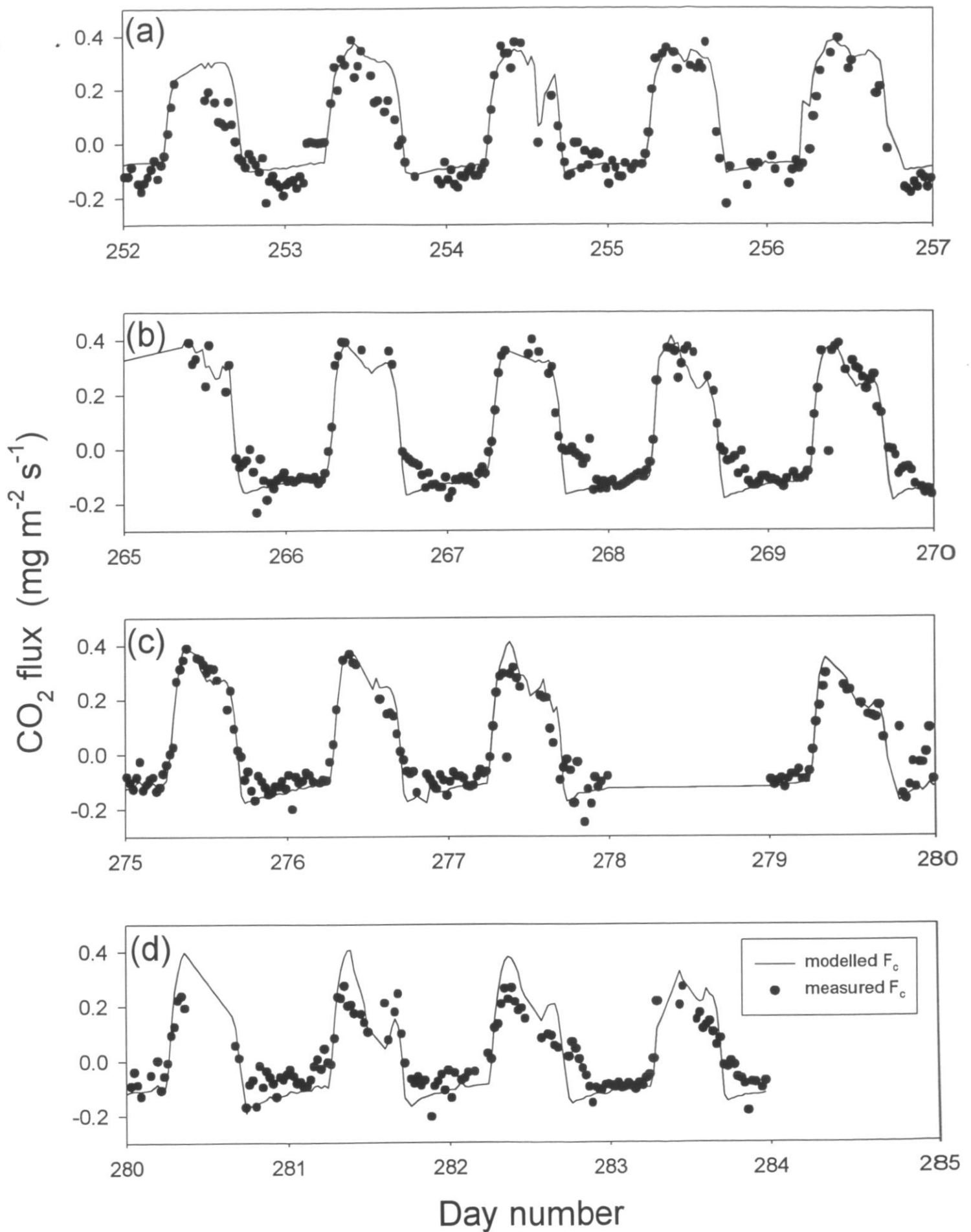


Figure 4. A comparison between measured (closed circles) and modelled (solid lines) total net CO₂ flux for a) days 252-256 (wet period), b) days 265-269 (just after the last rainfall), c) days 275-279 (dry-down), d) days 280-284 (start of senescence).

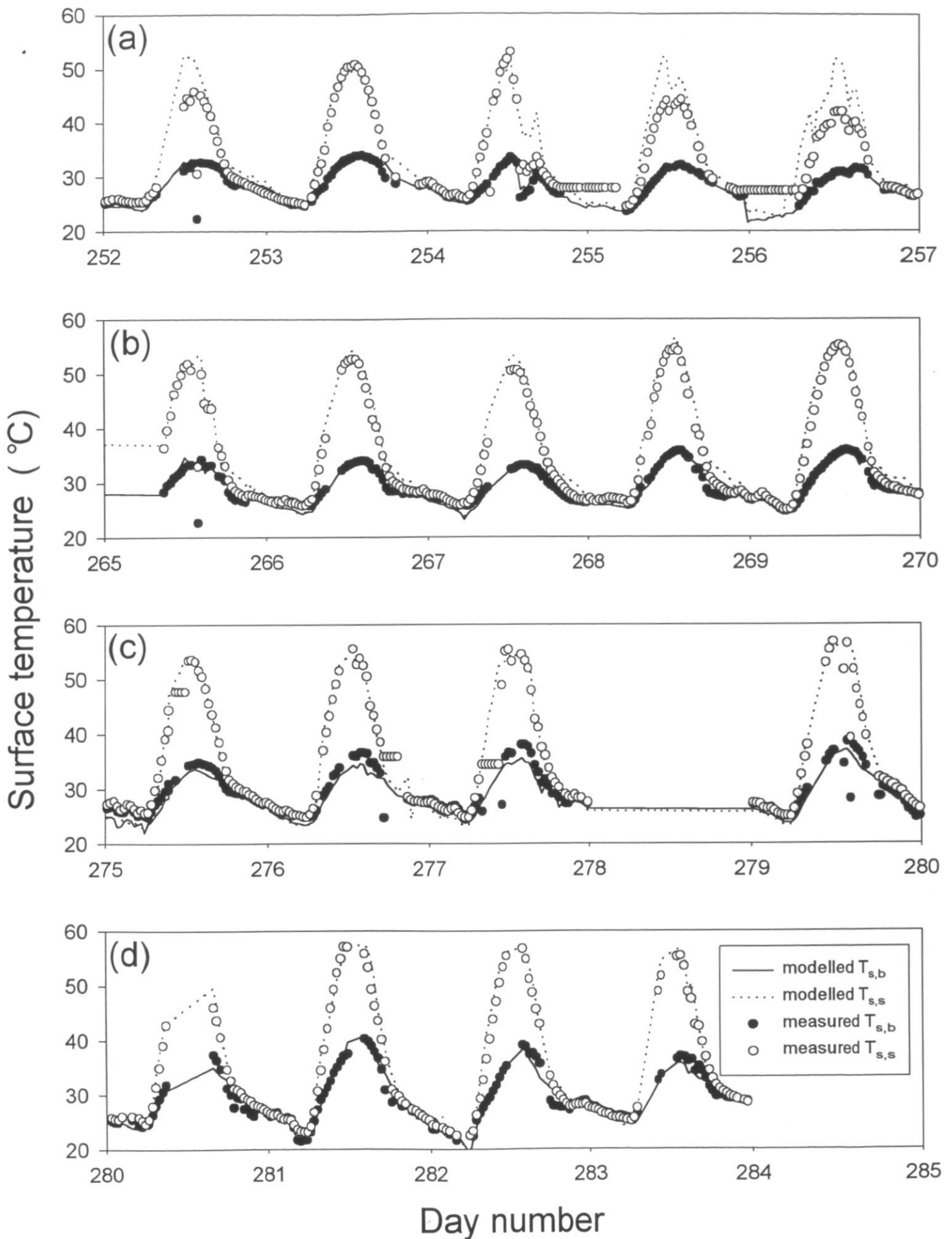


Figure 5. A comparison between measured (closed circles) and modelled (solid lines) bush surface temperature and measured (open circles) and modelled (dotted lines) soil surface temperature for a) days 252-256 (wet period), b) days 265-269 (just after the last rainfall), c) days 275-279 (dry-down), d) days 280-284 (start of senescence).

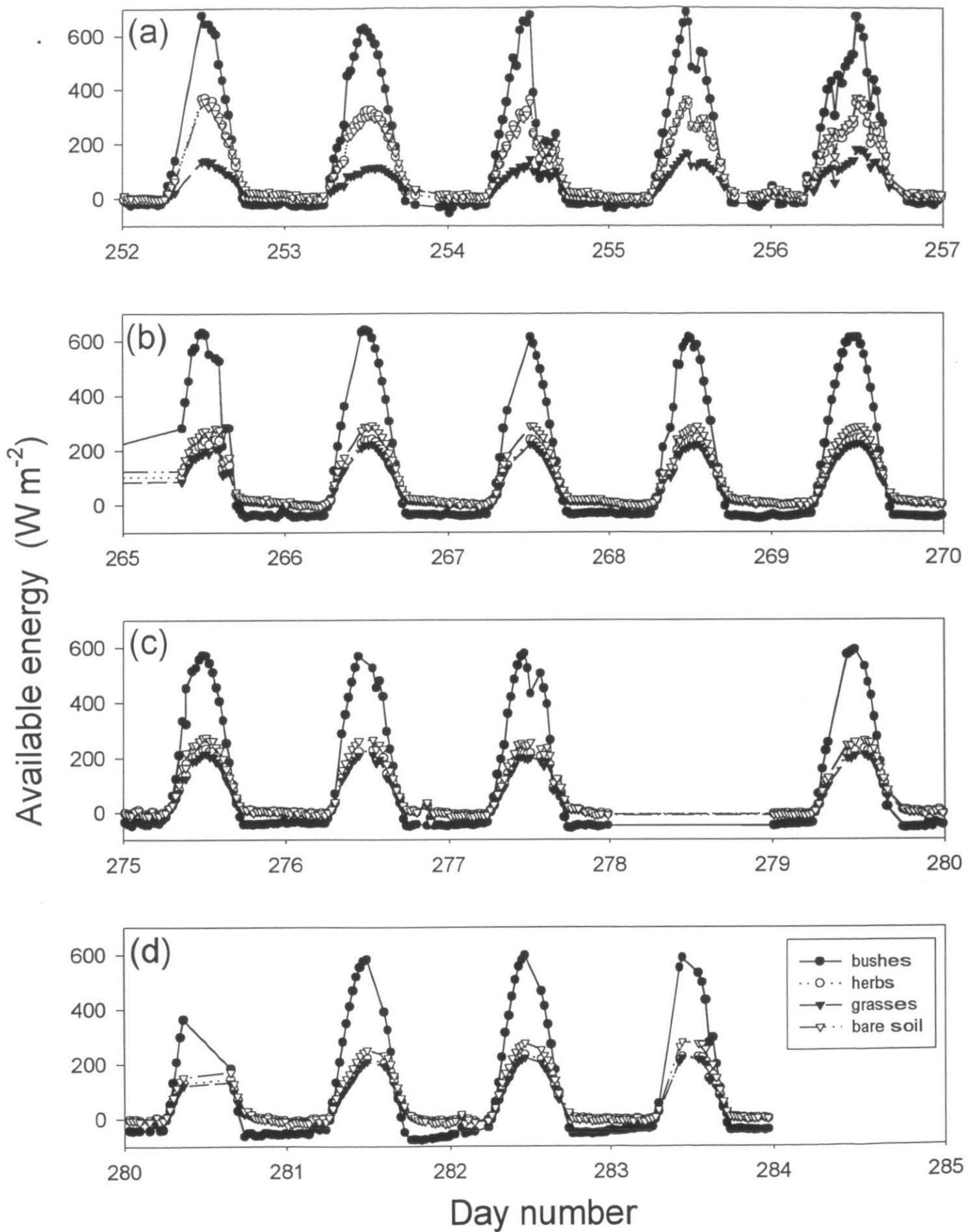


Figure 6. The course of the individual available energy for the four surface components during a) days 252-256 (wet period), b) days 265-269 (just after the last rainfall), c) days 275-279 (dry-down), d) days 280-284 (start of senescence).

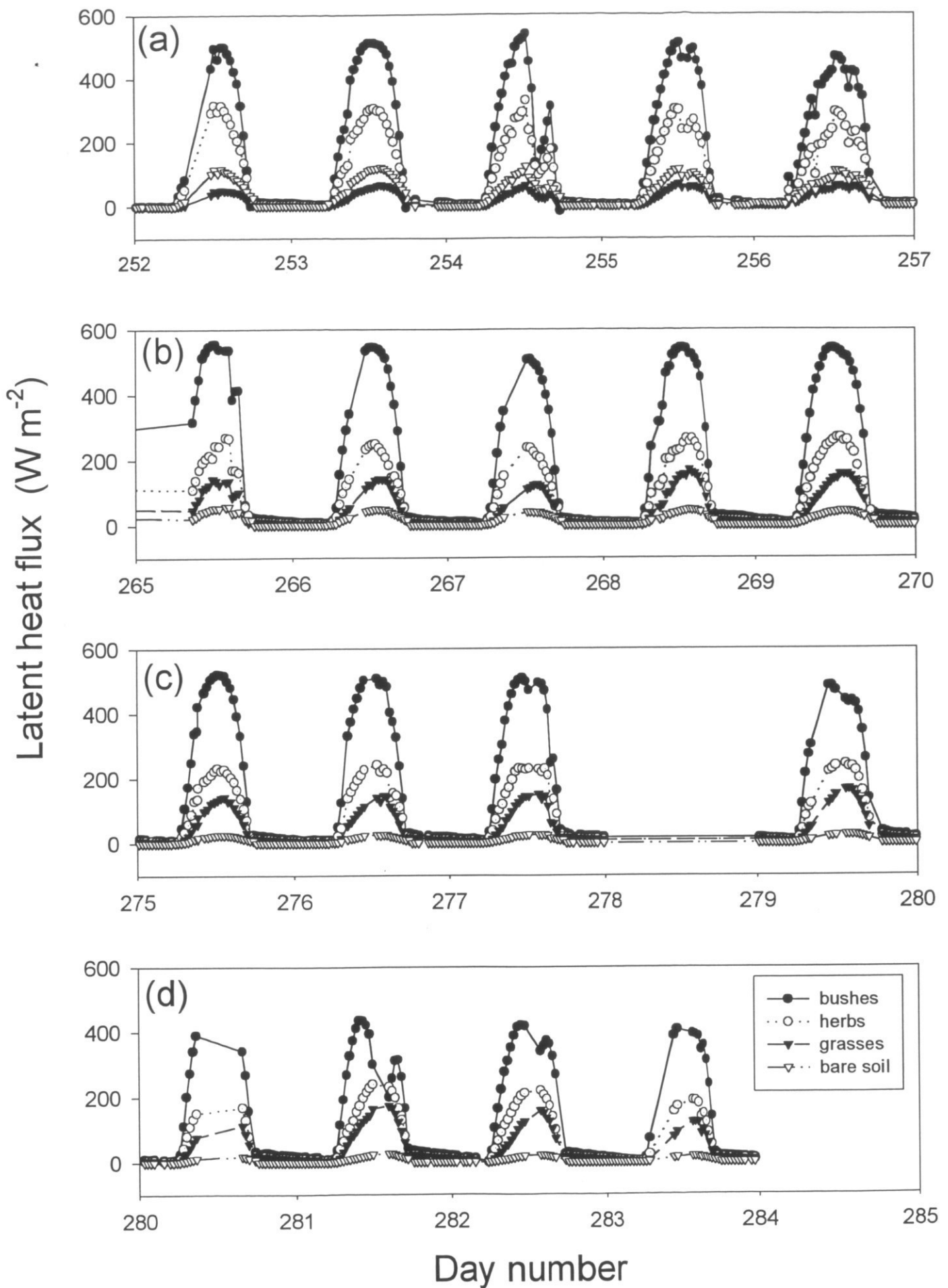


Figure 7. The course of the latent heat flux for the four surface components during a) days 252-256 (wet period), b) days 265-269 (just after the last rainfall), c) days 275-279 (dry-down), d) days 280-284 (start of senescence).

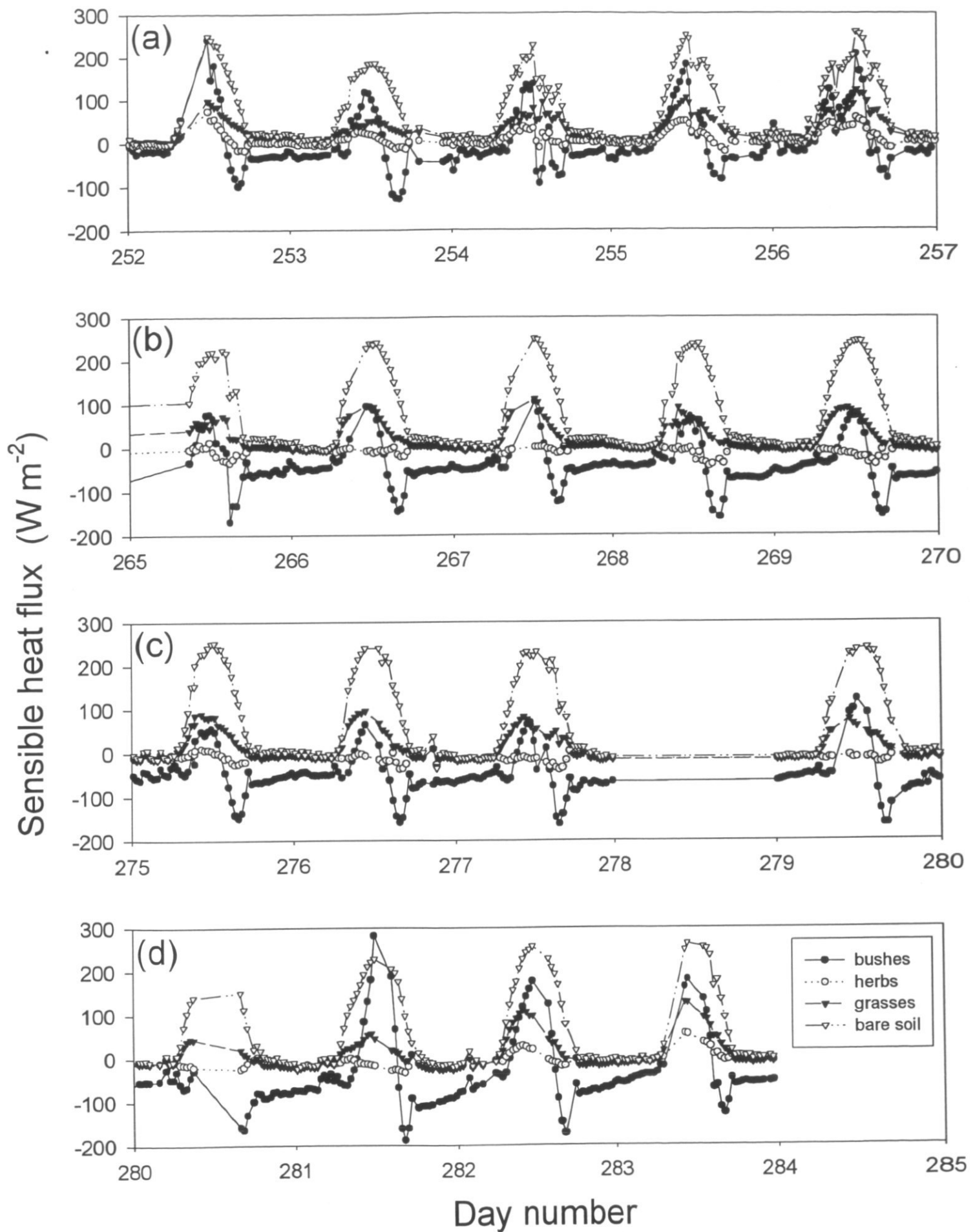


Figure 8. The course of sensible heat flux for the four surface components during a) days 252-256 (wet period), b) days 265-269 (just after the last rainfall), c) days 275-279 (dry-down), d) days 280-284 (start of senescence).

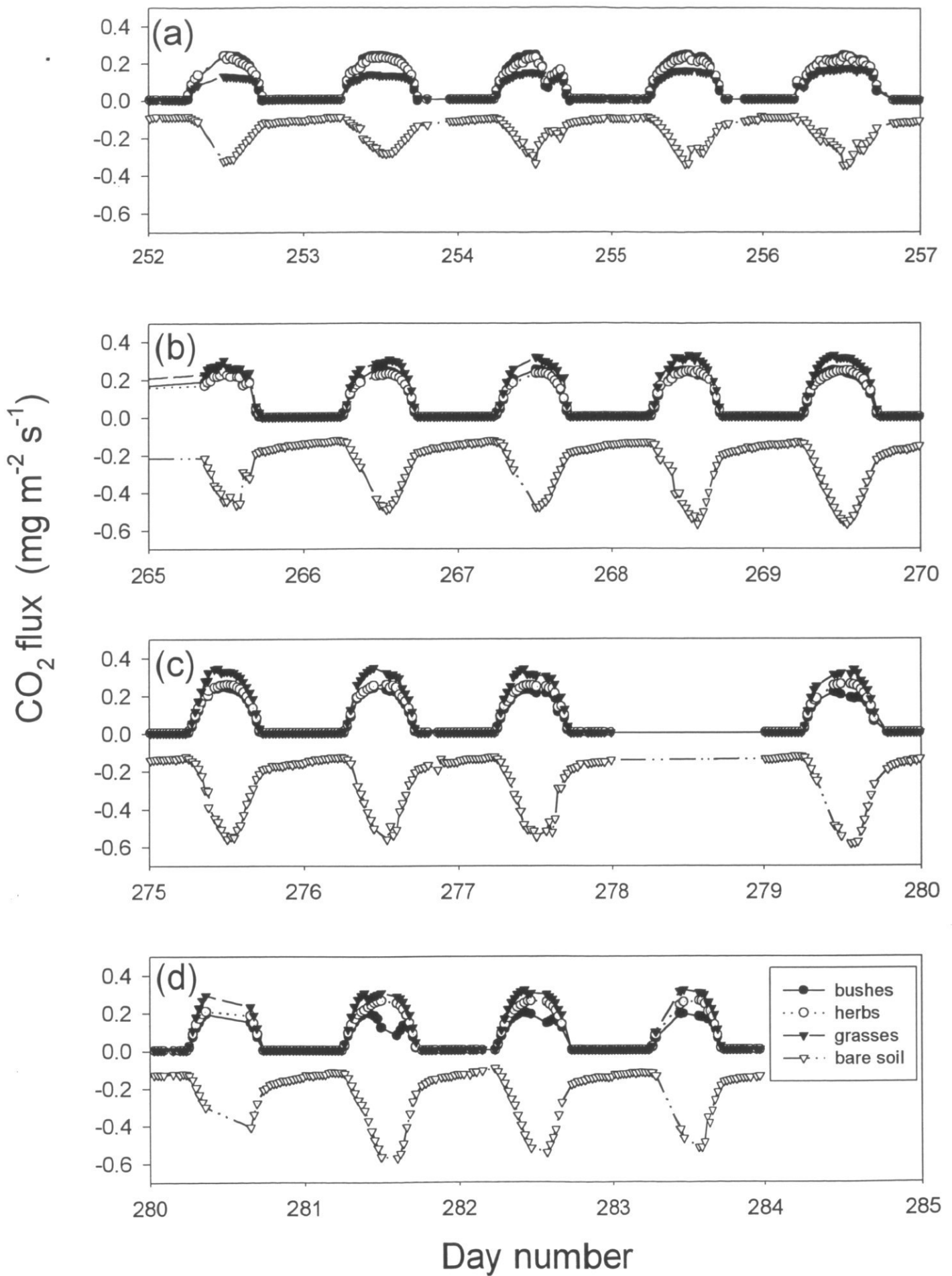


Figure 9. CO₂ exchange for the four surface components during a) days 252-256 (wet period), b) days 265-269 (just after the last rainfall), c) days 275-279 (dry-down), d) days 280-284 (start of senescence).

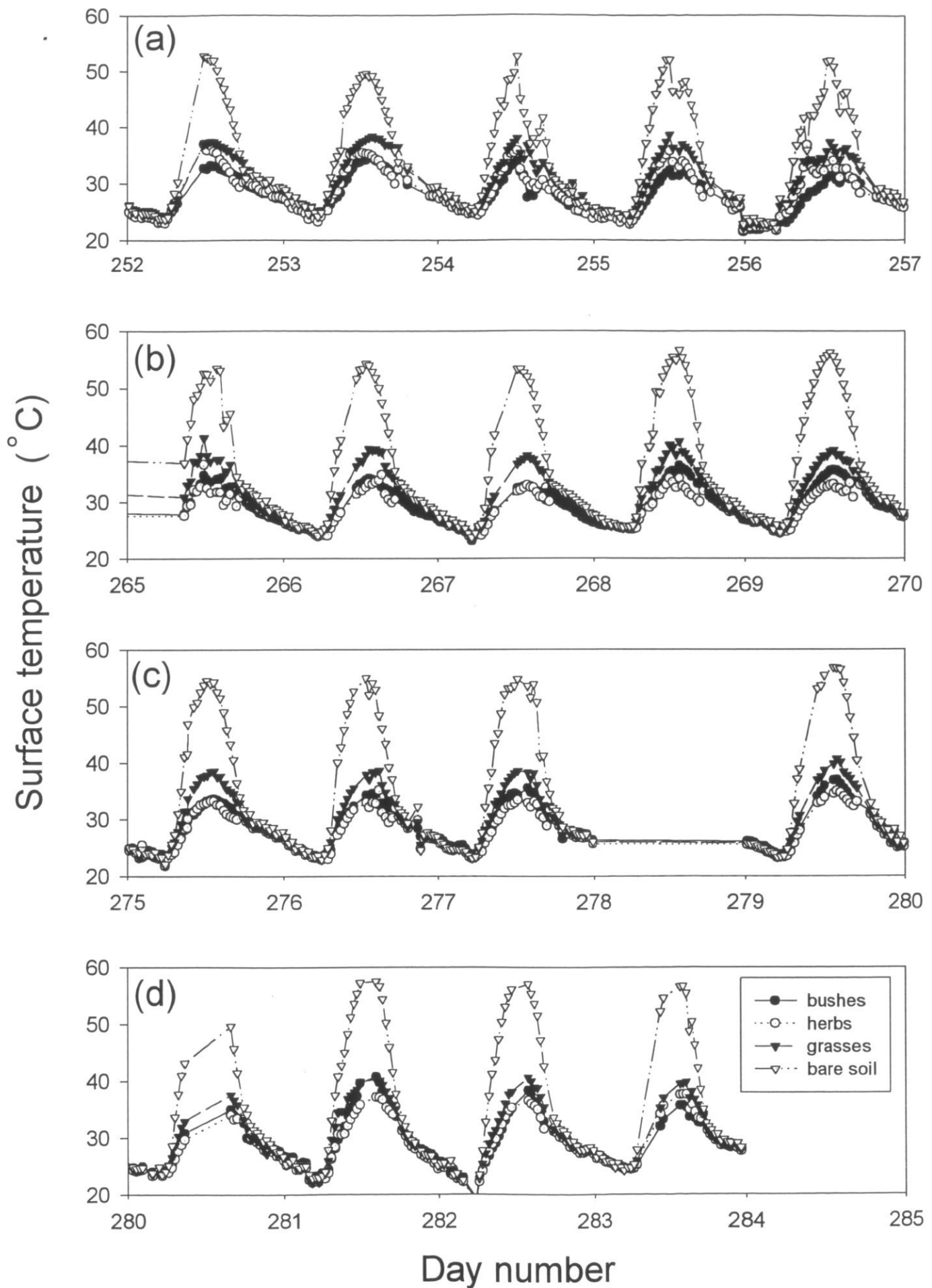


Figure 10. The course of surface temperatures for the four surface components during a) days 252-256 (wet period), b) days 265-269 (just after the last rainfall), c) days 275-279 (dry-down), d) days 280-284 (start of senescence).

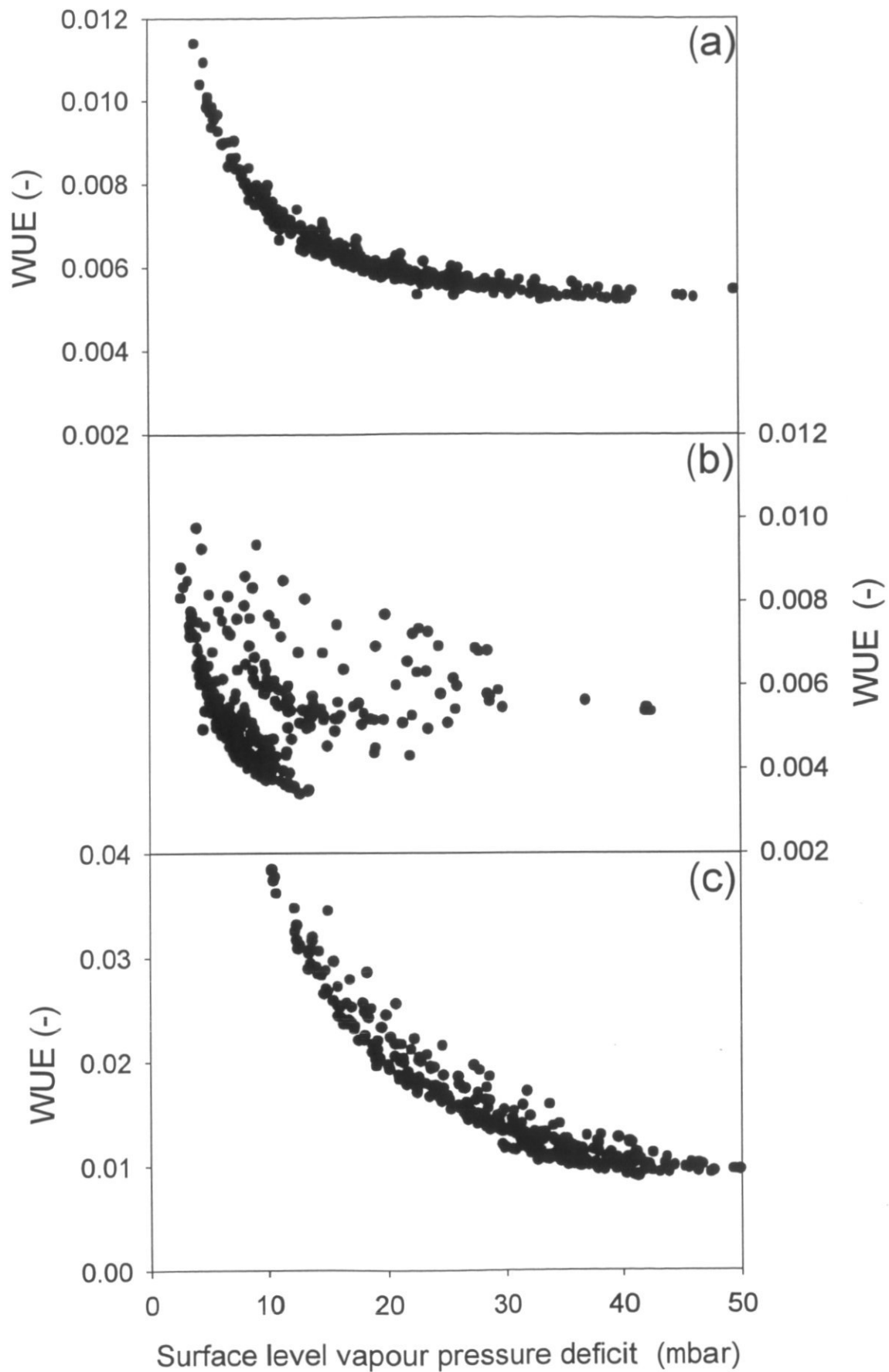


Figure 11. Water use efficiency (WUE) as a function of surface level vapour pressure deficit, $D_{s,i}$, for a) *Guiera senegalensis*, b) *Mitracarpus scaber* and c) *Digitaria guyana*.

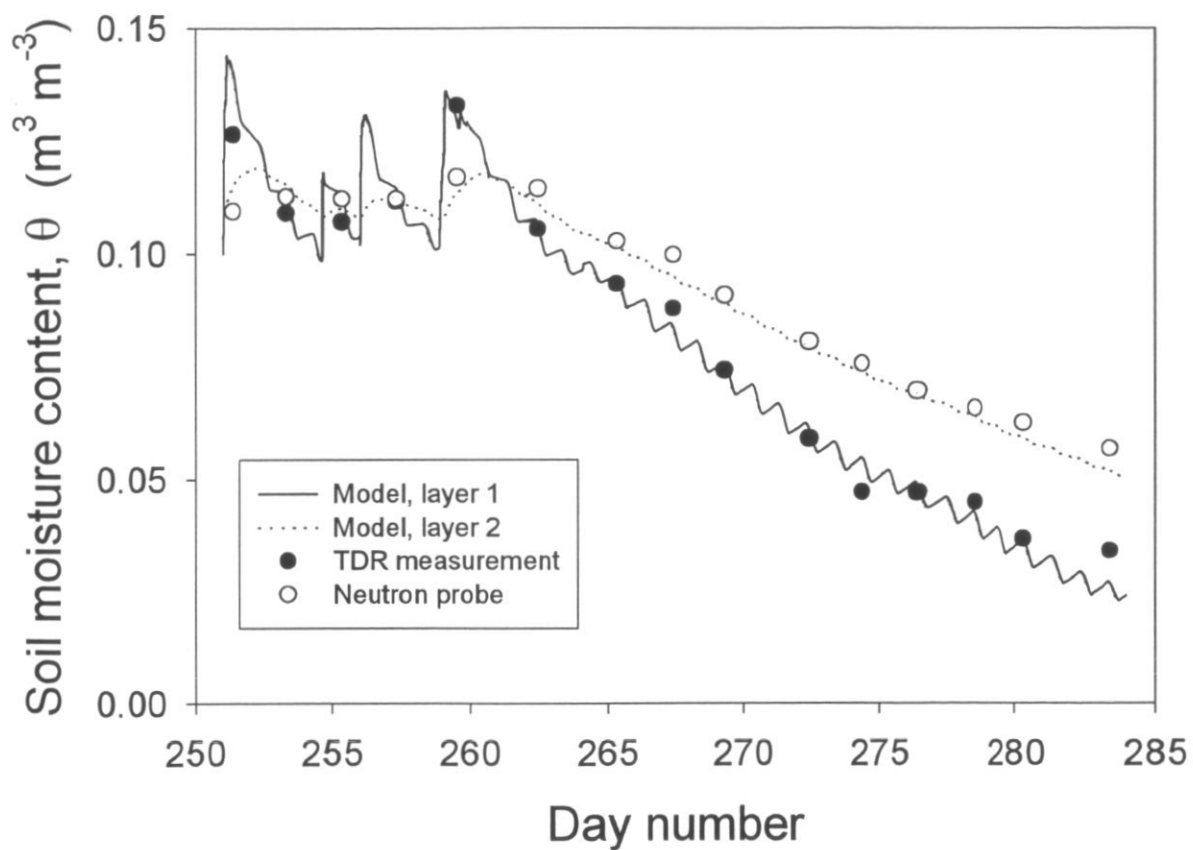


Figure 12. Measured (symbols) and modelled (lines) soil moisture content at two depths (-0.15 and -0.45 m, respectively) during the experimental period.

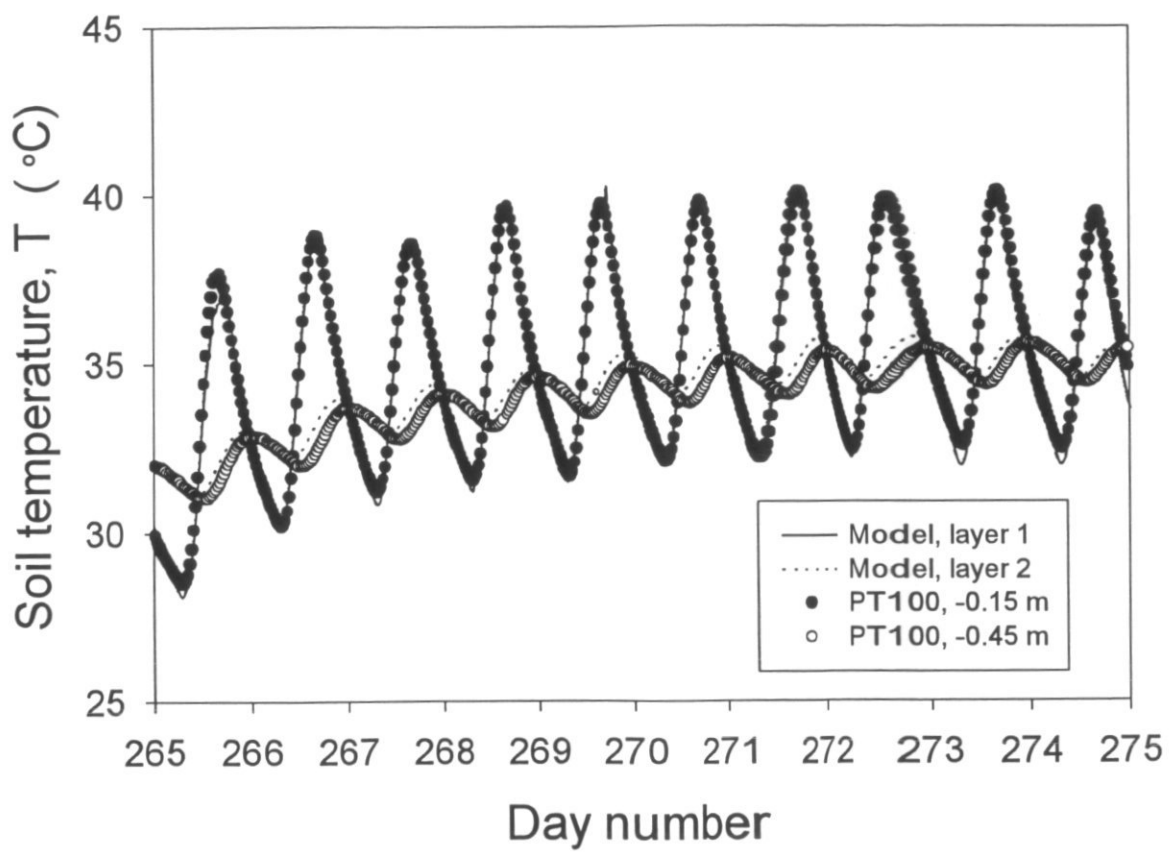


Figure 13. Measured (symbols) and modelled (lines) soil temperature at two depths (-0.15 and -0.45 m, respectively) during ten days of the experimental period.

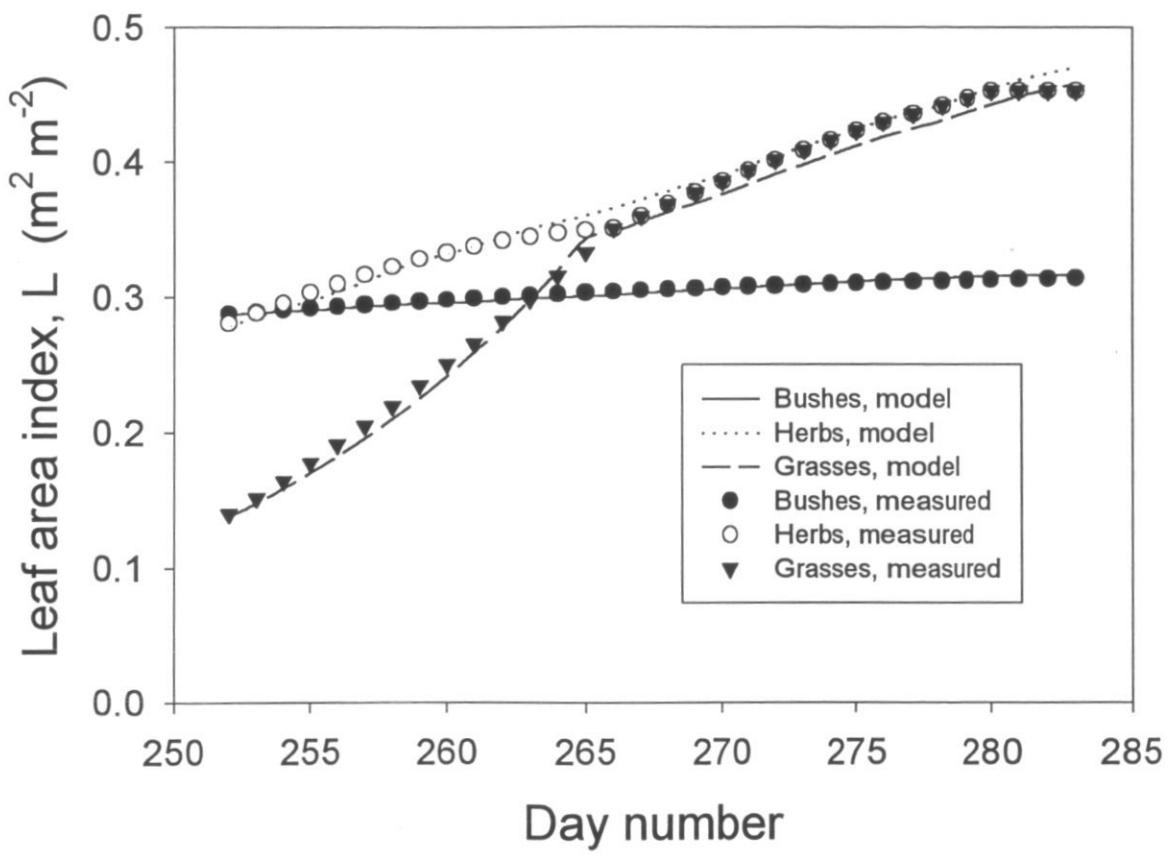


Figure 14. Measured (symbols) and modelled (lines) leaf area indices for the bushes, herbs and grasses, during the experimental period.

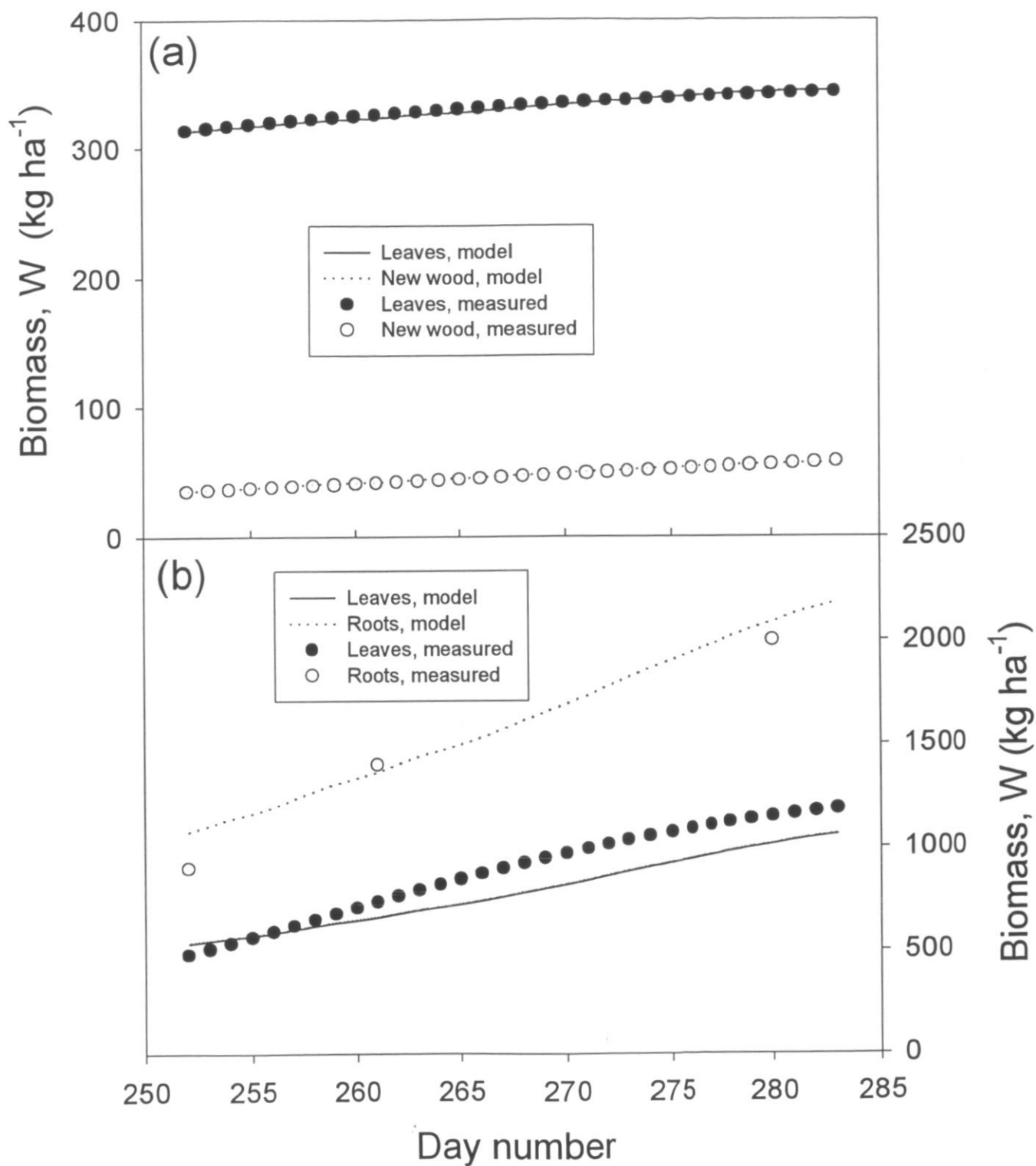


Figure 15. a) Measured (symbols) and modelled (lines) values of *Guiera* leaf and new wood biomass and b) measured (symbols) and modelled (lines) values of total herb layer leaf and root biomass and during the experimental period.

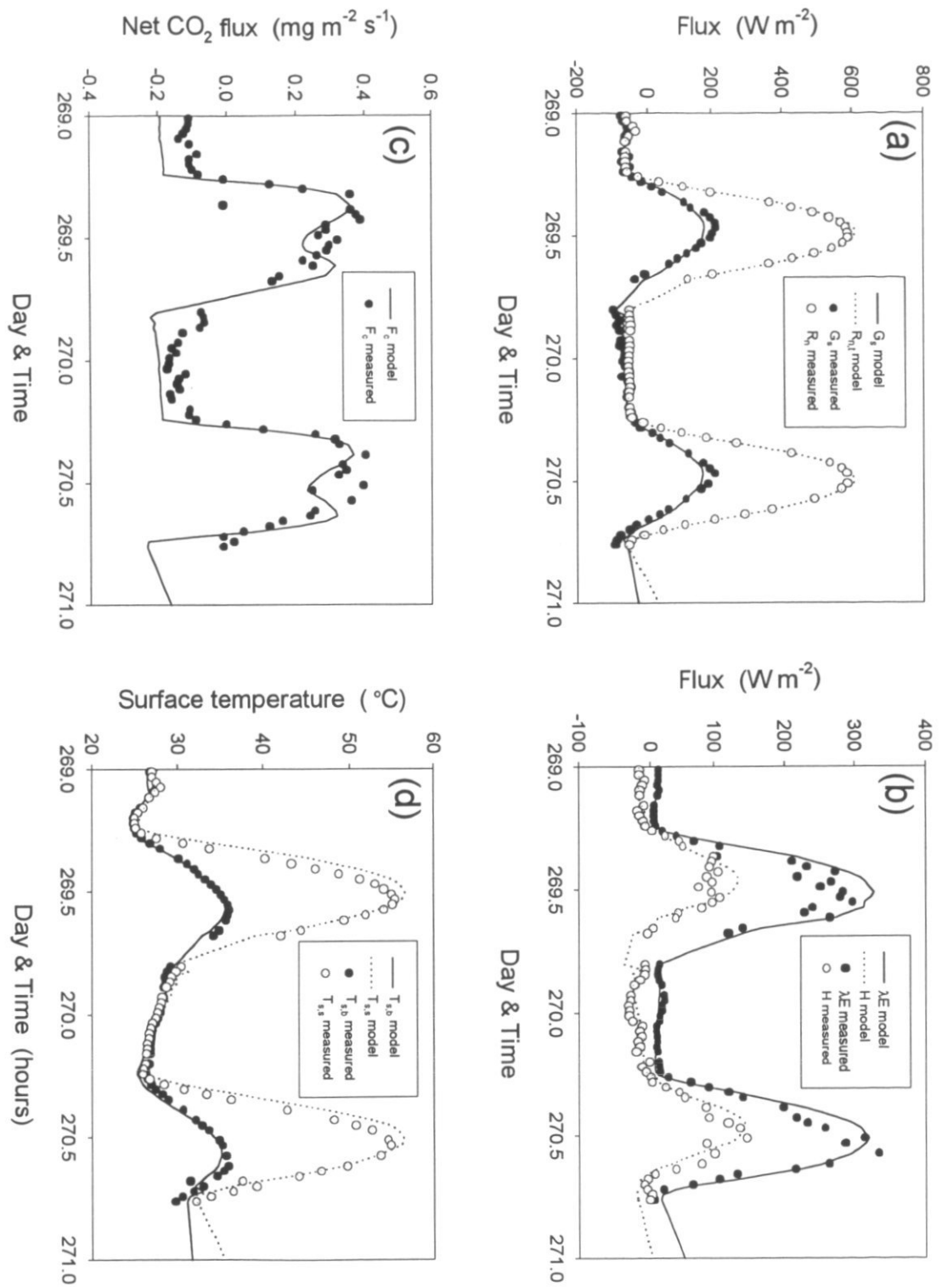


Figure 16. a) Measured (symbols) and modelled (lines) values of total net radiation and soil heat flux, b) of latent and sensible heat flux, c) of net CO_2 flux and d) bush and bare soil surface temperatures during two days of the experimental period.

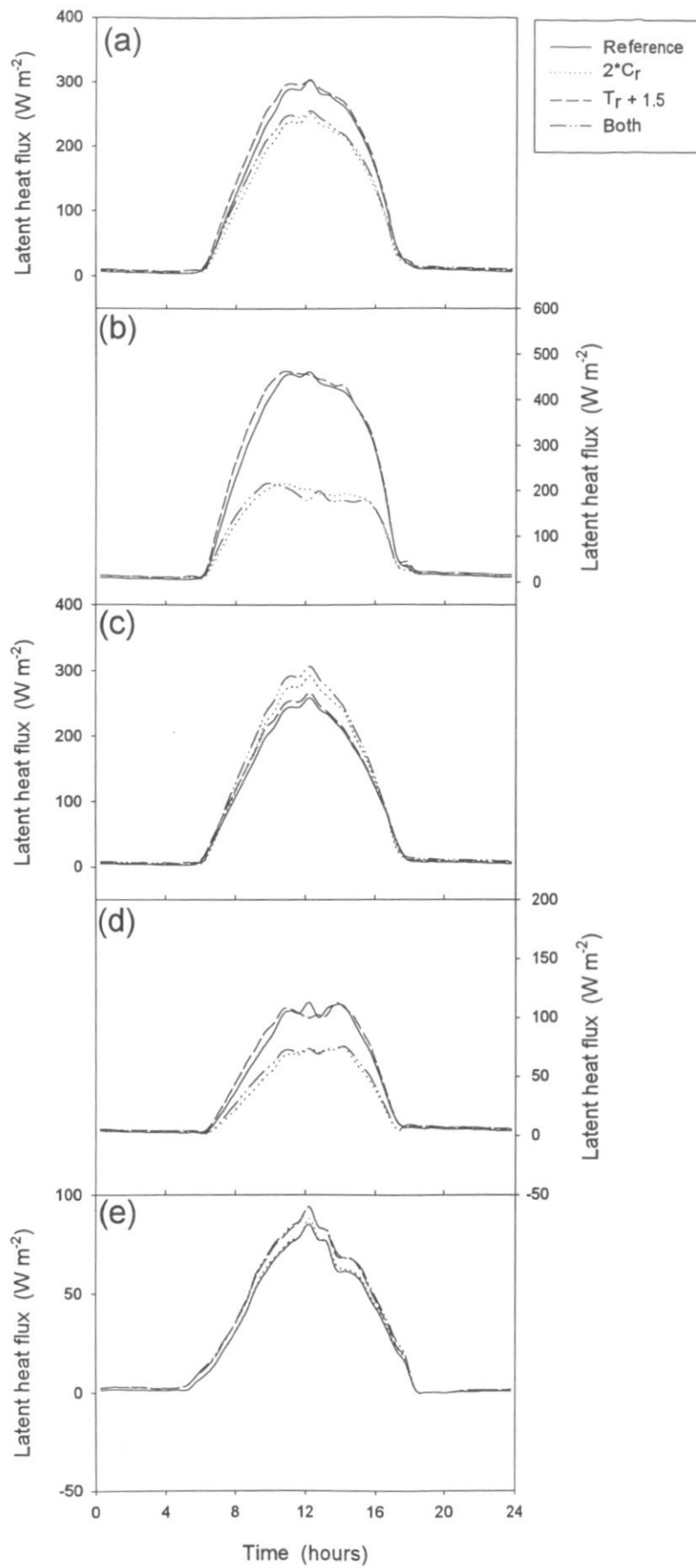


Figure 17. Average diurnal course of latent heat flux for a) the total savannah, b) bushes, c) herbs, d) grasses and e) bare soil calculated for four different climate change scenarios.

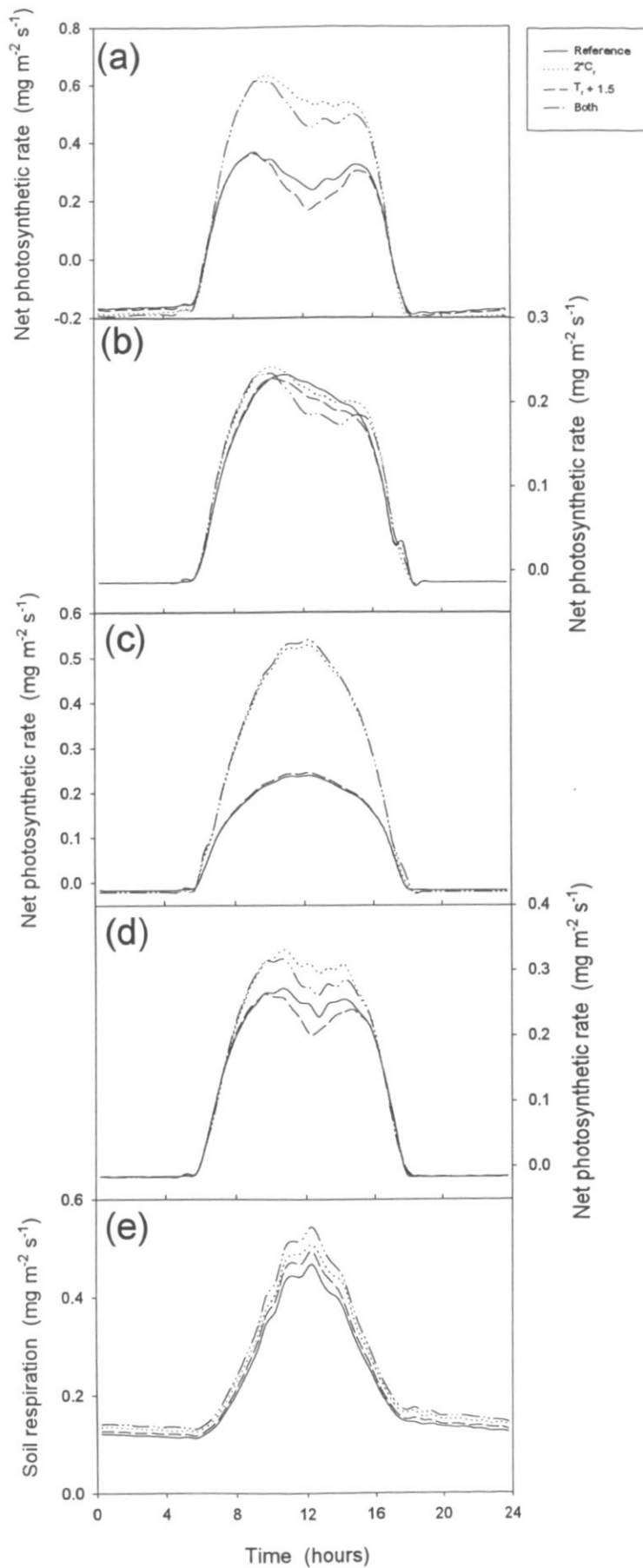


Figure 18. Average diurnal course of net photosynthetic rate for a) the total savannah, b) bushes, c) herbs, d) grasses and e) respiration for the bare soil calculated for four different climate change scenarios.

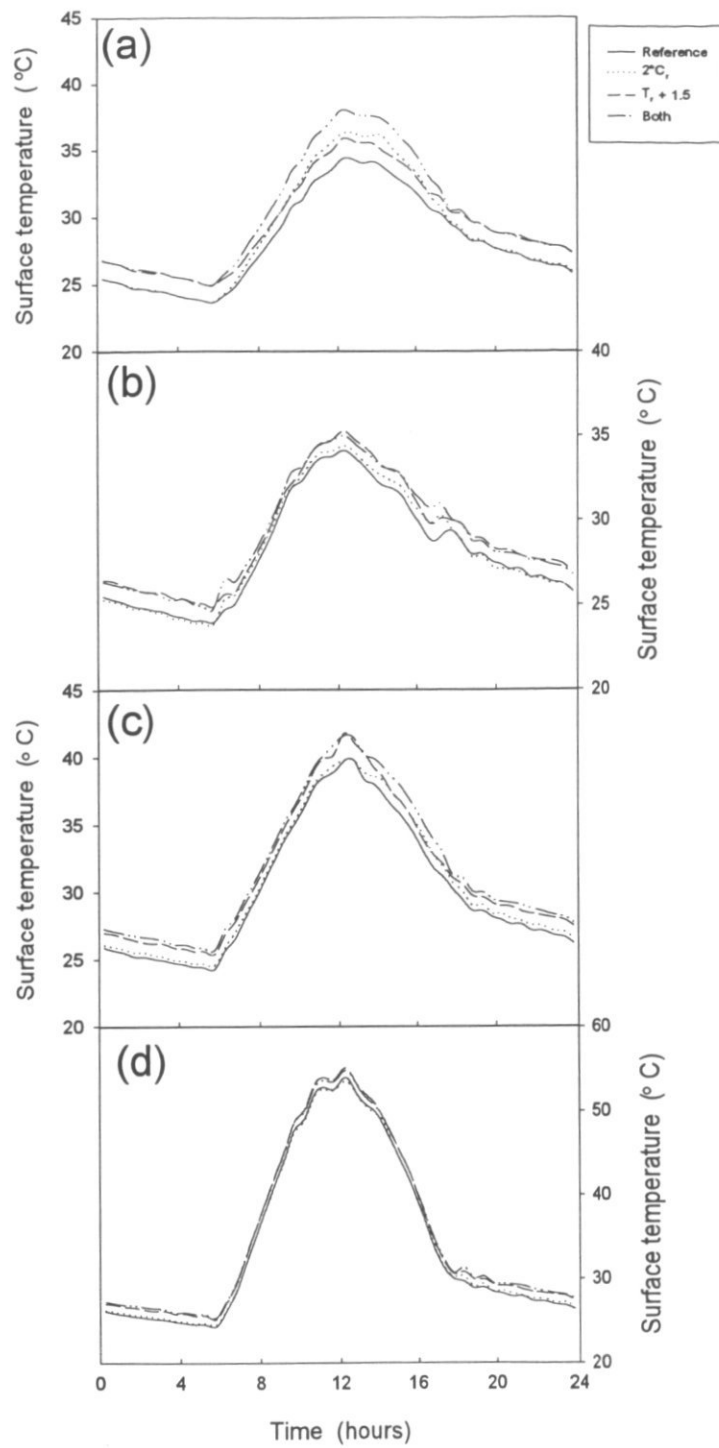


Figure 19. Average diurnal course of surface temperatures for a) bushes, b) herbs, c) grasses and d) bare soil calculated for four different climate change scenarios.

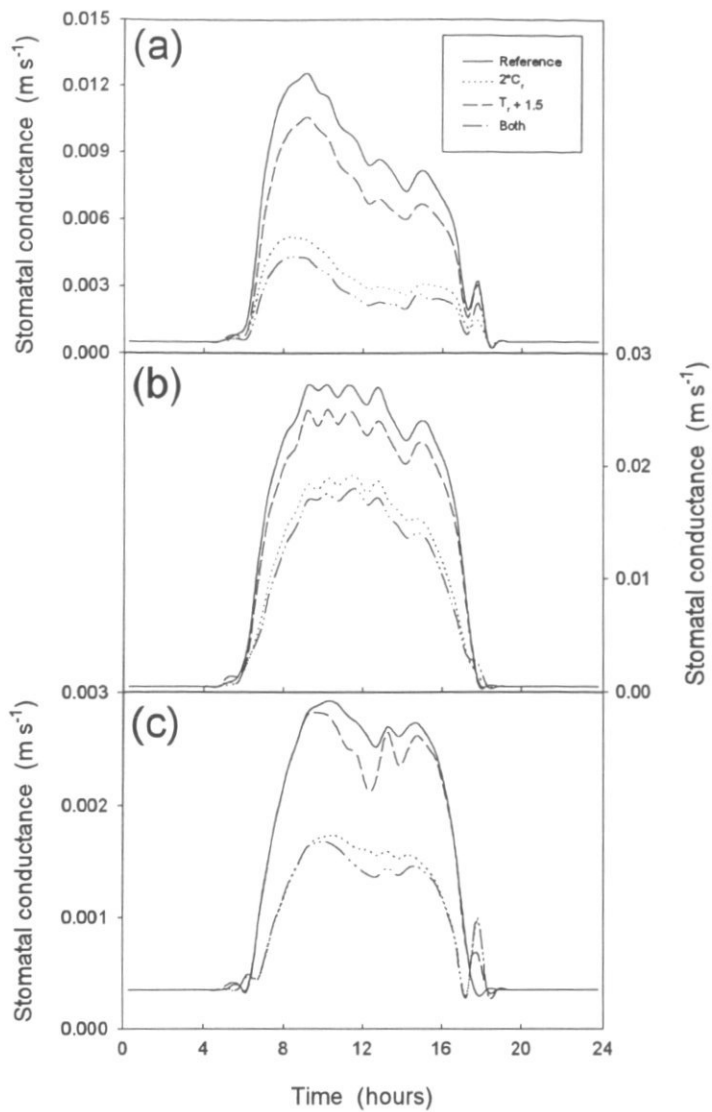


Figure 20. Average diurnal course of stomatal conductance for a) bushes, b) herbs and c) grasses calculated for four different climate change scenarios.

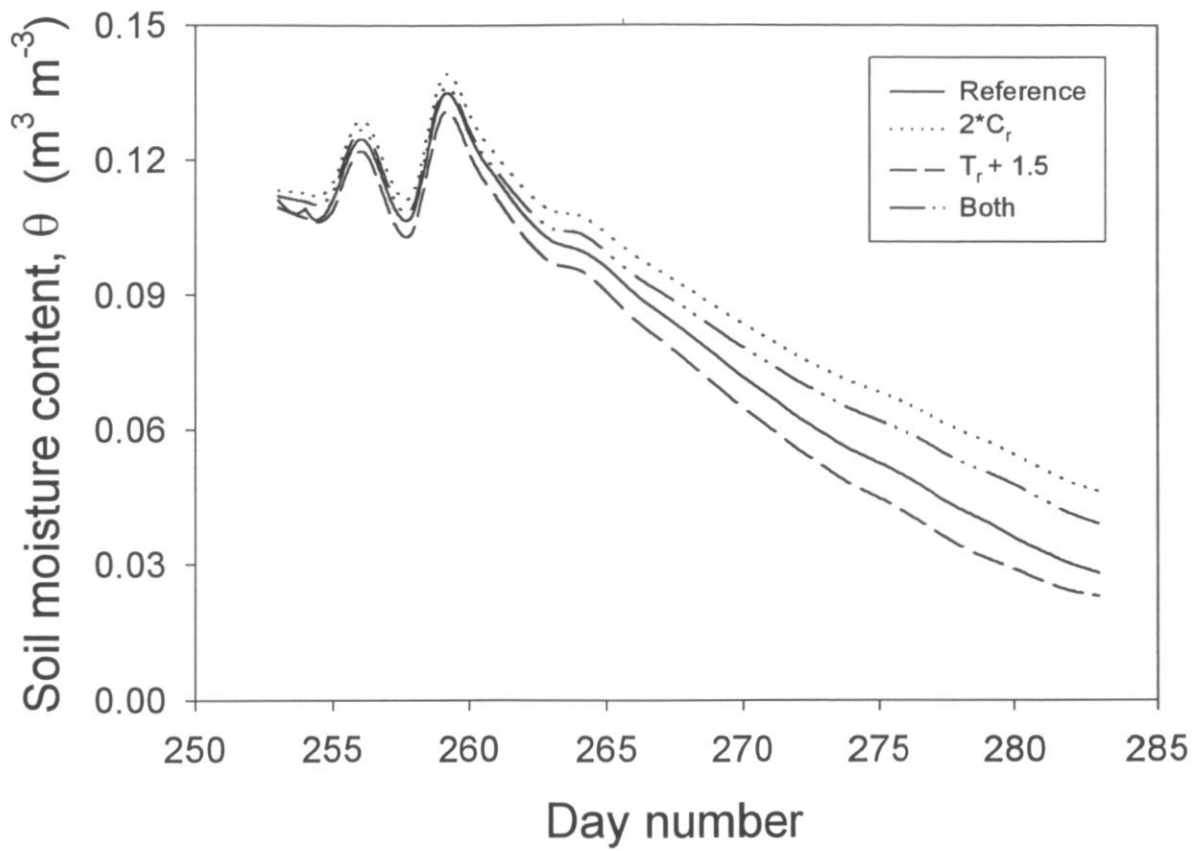


Figure 21. Daily averaged soil moisture content of the first soil layer (0-0.3 m) during the experimental period calculated for four different climate change scenarios.

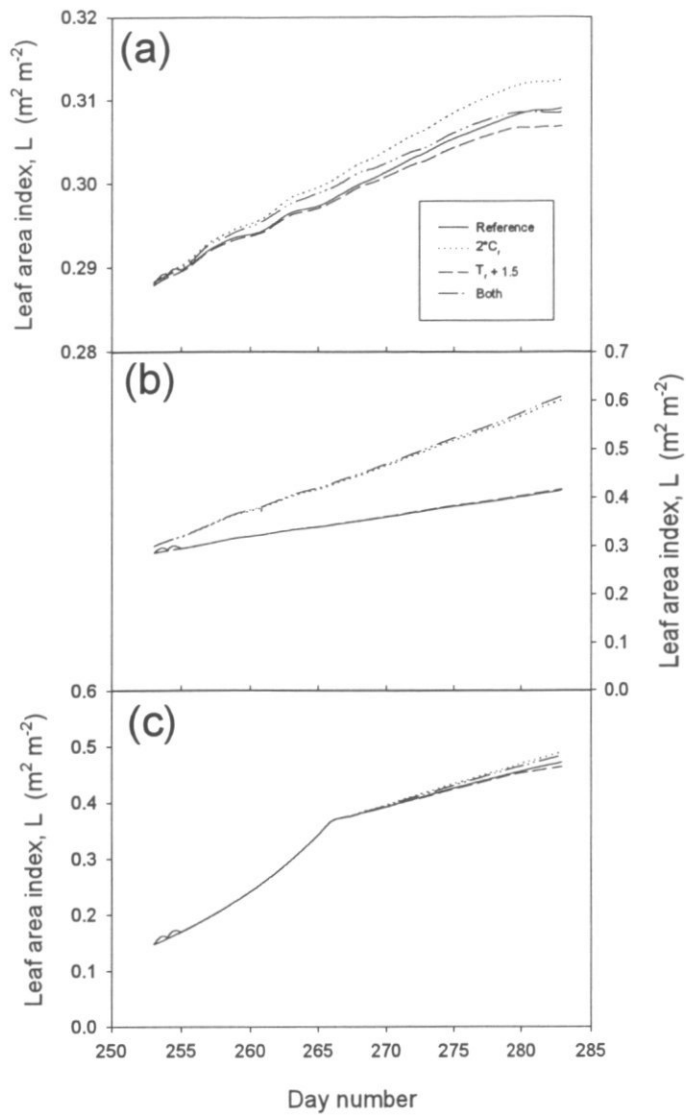


Figure 22. Leaf area index during the experimental period calculated for four different climate change scenarios for a) bushes, b) herbs and c) grasses.